On the stability and evolution of isolated molecular clouds

Richard P. Nelson[1]
Astronomy Unit, School of Mathematical Sciences, Queen Mary & Westfield College,
Mile End Rd, London, E1 4NS.

and

William D. Langer[2]
MS 169-506, Jet Propulsion Laboratory, California Institute of Technology, Pasadena, CA 91109

star formation

ABSTRACT

We present the results of three dimensional hydrodynamic models of evolving, isolated, low mass, quiescent clouds and Bok globules, where the **interstellar radiation** field plays an important role in the thermal and **chemical evolution**, and **thermal pressure** provides dominant support against gravitational collapse. The models are based on our earlier work with a Smoothed Particle Hydrodynamics code, but upgraded to include a larger chemical network, refined thermal, and dust properties, and different boundary conditions. The chemical network predicts the abundances of several key tracers of cloud structure and evolution including, C^+, CI, and CO. The chemical network, while limited in scope, keeps track of the major pools of the carbon and oxygen species such that these can be input into standard time dependent but static chemical codes to predict the abundances of less abundant trace species.

Calculations are performed for clouds, with masses in the range $M = 8$ to $60 M_\odot$, sizes in the range $R = 0.34$ to 1.8 pc, and with initial number densities in the range $50 \leq n \leq 1000$ cm^{-3}. The main purpose of these calculations is to calculate the effective 'Jeans masses' of the clouds, as a function of their initial number density, n. This was achieved by performing a parameter space search so as to locate the regions of stability and instability in the number density – mass plane.
The main results are:
(i) A subset of our calculations resulted in the formation of cold, dense, molecular cores that were gravitationally unstable, surrounded by warm, tenuous halos in which the trace species were in ionic or atomic form.
(ii) The evolution of these initially diffuse, isolated clouds, is driven at first by a pressure gradient through the cloud that arises because of the attenuation of the FUV

[1]R.P.Nelson@qmw.ac.uk

[2]langer@nimba.jpl.nasa.gov

component of the interstellar radiation field. Subsequent thermal evolution can lead to gravitational instability.
(iii) We find that the dense cores that arise in our simulations have masses in the range $3 \lesssim M \lesssim 20$ $M_\odot$, radii in the range $0.1 \lesssim R \lesssim 0.2$ pc, and have temperatures in the range $8 \lesssim T \lesssim 12$ K. These compare closely with the observationally derived properties of Bok globule cores.
(iv) The characteristics of the collapsing, dense cores are similar to those of collapsing, isothermal spheres, since the gas evolves towards a constant temperature of 10 K before collapse ensues.

Subject headings: molecular clouds: dynamics — stars: formation

1. Introduction

Isolated, low mass clouds, such as Bok globules, are some of the simplest objects capable of forming stars. As such they are important objects for both observational and theoretical study. A number of observational studies of these clouds have appeared in the literature over recent years. Clemens & Barvainis (1988) compiled a catalogue of 248 nebulae from the POSS plates, and 244 of these objects were detected in the CO ($J = 2 \rightarrow 1$) transition by Clemens, Yun, & Heyer (1991). A similar catalogue of 169 objects was compiled by Bourke, Hyland, & Robinson (1995), and a follow–up ammonia survey detected about half of these (Bourke *et al.* 1995), indicating the presence of dense gas. Approximately half the clouds were found to have IRAS sources lying towards them, with colors typical of embedded objects. Similar statistics arise from the work of Clemens & Barvainis (1988).

Many of these objects have been observed in the submillimetre continuum (Launhardt, Ward–Thompson, & Henning 1997), in the millimetre continuum (Launhardt & Henning 1997, Henning & Launhardt 1998), and in the high density gas tracer CS (Henning & Launhardt 1998, Launhardt *et al.* 1998), as well as the radio continuum (Yun *et al.* 1996). These observations indicate that dense gas is ubiquitously associated with embedded, protostellar sources (Class 0 and Class I), and that the Bok globules, as a population, are sites of active star formation. Many of these globules appear to contain outflows (Yun & Clemens 1994b, Henning & Launhardt 1998), further bolstering the evidence for on–going star formation activity in these isolated clouds. In addition, there exists a population of 'starless globules', which lack evidence for embedded sources, but contain dense, molecular cores. These may either be clouds which have, or will fail, to make stars, or else be clouds which are in a pre protostellar state. The basic physical properties of Bok globule molecular cores are such that their masses are typically in the range $0.1 \lesssim M \lesssim 50$ $M_{\odot}$, cold gas temperatures of $T \simeq 10$ K, and sizes on the order of $R \sim 0.1 - 0.3$ pc. In addition, some, but not all of these globules, appear to be quiescent, with line widths indicating motions that are approximately sonic or subsonic (Clemens & Barvainis 1988). Outside of the dense molecular region, there is probably a more tenuous halo region, which may nonetheless contain a substantial amount of matter. The halo is more difficult to study because the primary tracers of this gas, CI, C^+, and OI are harder, or impossible, to observe from the ground.

In view of the growing body of evidence for on–going star formation in these clouds, it seems timely to undertake a theoretical study of these objects. In a previous paper (Nelson & Langer 1997, hereafter NL97), we presented some simple calculations of evolving clouds that were externally heated by the FUV component of the interstellar radiation field (ISRF), were able to cool through line emission, and which contained a highly simplified treatment of the chemistry. We have now substantially alterted the treatment of the chemistry, and extended our modeling of the clouds' thermal evolution. Here we present a numerical stability analysis of isolated, thermally supported, low mass clouds, in order to ascertain the effective 'Jeans masses' of such objects, employing the smoothed particle hydrodynamics (SPH) code described in NL97. Although our calculations neglect the effects of turbulence and magnetic fields, which we hope to include in

subsequent work, we believe that these calculations shed some interesting light on how such low mass clouds may evolve to form stars.

The clouds that we have modeled are typically in the mass range $8 \leq M \leq 60$ $M_{\odot}$, are of uniform density initially with number densities in the range $50 \leq n \leq 1000$ cm^{-3}, and have sizes $0.34 \leq R \leq 1.8$ pc. In their initial state, the clouds are gravitationally stable with values of α, the ratio of the thermal to gravitational potential energy being typically $\alpha \sim 2$ –6. It is found, however, that the clouds are able to evolve from an initially diffuse state, to one in which the cloud develops a distinctive core–halo stucture, with a cold, dense, gravitationally unstable core, surrounded by a warm, tenuous halo. This evolution is largely driven initially by the existence of a pressure gradient which is set up in the cloud because of the attenuation of the FUV component of the ISRF. The subsequent thermal, chemical, and dynamical evolution allows the cloud to form a gravitationally unstable core in a subset of the calculations that we have performed. The role played by the chemistry in these calculations is two–fold. First, the conversion of one chemical species to another changes the thermodynamic evolution of the cloud since different species cool at different rates. Second, the chemistry determines which atomic, ionic, and molecular species are the best tracers of different parts of the cloud. The thermal evolution of the cloud allows the inner regions to cool as the density increases there, and thus to evolve to a state of gravitational instability.

The paper is organized as follows. The physical model that we assume, including the basic equations, the thermal model, the chemical model, and the numerical method we employ are described in section (2). The initial and boundary conditions are described in section (3), and the results of our calculations are described in section (4). A discussion is presented in section (5), including a comparison between the calculations and relevant observations, and conclusion are drawn in section (6).

2. The Physical Model

In the following sections we provide a brief description of the various physical processes that we have included in our models of isolated molecular clouds. The reader is referred to NL97 for a detailed description of the heating and cooling processes included in our models. We have added some improvements to our thermal model, and substantially altered our description of the chemistry. These changes are described below.

2.1. Basic Equations

The continuity, momentum, and energy equations for a compressible fluid can be written

$$\frac{d\rho}{dt} + \rho \nabla . \mathbf{v} = 0 \tag{1}$$

$$\frac{d\mathbf{v}}{dt} = -\frac{1}{\rho}\nabla P - \nabla\Phi + \mathbf{S}_{visc} \tag{2}$$

$$\frac{d\mathcal{U}}{dt} + \frac{P}{\rho}\nabla.\mathbf{v} = \frac{\Gamma - \Lambda}{\rho}. \tag{3}$$

where

$$\frac{d}{dt} = \frac{\partial}{\partial t} + \mathbf{v}.\nabla \tag{4}$$

denotes the convective derivative, ρ is the density, $\mathbf{v}$ is the velocity, P is the pressure, $\mathbf{S}_{visc}$ represents the viscous forces, $\mathcal{U}$ is the internal energy per unit mass, and Φ is the gravitational potential. Both Γ and Λ represent non adiabatic heating and cooling processes, respectively. The chemical rate equation is written in the usual form

$$\frac{dX_i}{dt} = nK_i \tag{5}$$

where X_i is the fractional abundance of chemical species i, K_i is the associated chemical reaction rate, and n is the total number density. This set of equations is supplemented by an equation of state, which for a perfect gas may be written

$$P = \frac{\mathcal{R}}{\mu}\rho T = K(S)\rho^{\gamma}, \tag{6}$$

where $\mathcal{R}$ is the gas constant, μ is the mean molecular weight, T is the temperature, $K(S)$ is a function of the entropy, and γ is the ratio of the specific heats. The models considered in this paper are largely for low temperature clouds, so that the kinetic temperature is below that necessary to excite the rotational and vibrational states of H_2. Thus, we take the value $\gamma = 5/3$. Higher temperatures may result in the outer envelopes of our cloud models, in which case γ will locally differ from 5/3. We are primarily interested in the gravitational stability of the cooler, denser regions that develop in the models, and do not believe that this should be substantially altered by changes to γ in the outer layers.

2.2. The Thermal Model

The thermal model that has been incorporated in the work presented here is largely based upon the calculations of Goldsmith & Langer (1978), along with some modifications and extensions that allow us to calculate the thermodynamics of initially diffuse molecular clouds more realistically. The details of the model used in the calculations presented here have largely been described in NL97. We have made some modifications, however, which we will describe below.

2.2.1. The Cooling Functions

The cooling is provided by molecular line cooling, and by the fine structure emission of OI, CI, and CII. The molecular line cooling is provided by an analytical fit to the cooling functions of Goldsmith & Langer (1978), and was described in NL97. The cooling functions adopted for the OI and CII were similarly described in NL97. The extensions to our chemical model now allow us to include the cooling due to CI, whose cooling rate is given by the equation:

$$\Lambda_{CI} = 1.38 \times 10^{-16} \left(e_{10} A_{10} f_1 \beta_{01} + e_{21} A_{21} f_2 \beta_{21}\right) n(CI) \quad \text{ergs cm}^{-3}\ \text{s}^{-1} \tag{7}$$

where A_{10} and A_{21} are the Einstein A coefficients, e_{10} and e_{21} are the energy differences between the levels, f_1 and f_2 describe the fractional level populations, β_{01} and β_{12} are the escape probabilities, and $n(CI)$ is the number density of CI. The fractional populations are calculated from the rate equations utilizing collision rate coefficients and A_{ul} from Genzel (1991). The escape probability is given by the usual expression, $\beta = (1 - exp(-\tau))/\tau$. The linewidth gradient is assumed to be 1 km s^{-1} pc^{-1}.

Cooling is also provided by gas–dust thermal exchange when the dust temperature is below the local gas temperature. Heating is provided when the converse is true. The gas–dust thermal coupling is described in NL97, with the modification that the dust temperature is calculated using the formula suggested by Hollenbach, Takahashi, & Tielens (1992). We note that this dust model predicts excessively low dust temperatures in our calculations when the central densities become high, so we set a minimum value of the dust temperature of $T_d = 10$ K.

2.2.2. The Heating Functions

The heating of the gas is primarily provided by the photoelectric emission of electrons from grains caused by the incident FUV (6 – 13.6 eV) component of background star light. We have modified the photoelectric heating term used in NL97 to include the effects of grain charging on the grain work function. The heating rate is now given by:

$$\Gamma_{pg} = 4.86 \times 10^{26} G_0 n f(T, n(e), \tau_{uv}) e^{-\tau_{uv}} \quad \text{ergs cm}^{-3}\ \text{s}^{-1} \tag{8}$$

where $f(T, n(e), \tau_{uv})$ is a factor which accounts for the effects of grain charging (Hollenbach, Takahashi, Tielens 1992), and G_0 is a factor which determines the flux of FUV radiation relative to the standard interstellar value ($G_0 = 1$) as reported by Habing (1968). The implementation of this heating term in our SPH code is described in detail in NL97.

Heating of the gas is also provided by cosmic ray ionization and H_2 formation on grains, as described in NL97. These heating processes provide the dominant contribution in the shielded, interior regions of the clouds.

2.3. The Chemical Model

The chemical model employed in NL97 assumed that the cloud was composed of molecular hydrogen with trace quantities of carbon and oxygen. A simplified chemical network was then employed to convert directly between C^+ and CO, in which the intermediate reactions were parameterized. We have augmented this chemical model substantially (see Appendix A for details), and now explicitly solve for the following species: He^+, H_3^+, OH_x, CH_x, CO, C, C^+, HCO^+, O, M, M^+, and e^-. We have grouped the species O_2, H_2O, and OH together into a composite species OH_x for the sake of keeping the chemical network at a manageable size. We have similarly grouped the hydrides CH and CH_2 into CH_x, and have introduced the species M to describe the metals Mg, Fe, Ca, and Na which provide a background source of electrons in the shielded regions of our clouds. These simplifications are justifiable on physical grounds because the species involved follow similar chemical pathways and react at similar rates. The results compare favorably to the 1-D hydrodynamical calculations of Shematovich *et al.* (1997) who used the complete UMIST chemical network but limited to at most diatomic molecules. In 1-D the transitions from C^+ to CI and CO, and OI to OH, H_2O, and O_2 in our models follows their results.

The reactions contained in our network, and their associated reaction rates, are listed in an Appendix. The reaction network consists of ten reactions in total, and is solved using the LSODE routine developed to handle sets of stiff equations.

2.4. Numerical Method

The set of equations described in the preceding sections are solved using smoothed particle hydrodynamics (Lucy 1977; Gingold & Monaghan 1977). SPH uses particles to represent a subset of the fluid elements that arise in the Lagrangian description of a fluid. The version of SPH used in the calculations presented here is a conservative formulation of the method that employs variable smoothing lengths (Nelson & Papaloizou 1994). In NL97 we highlighted those points salient to the work presented in this paper. A detailed description of the code is presented in Nelson & Papaloizou (1994), along with a number of test calculations. The number of particles used in each of the calculations described was $N = 28,421$, though higher resolution test calculations employing $N = 100,000$ particles were also performed to test for numerical convergence.

3. Initial and Boundary Conditions

The clouds considered in this paper are all spherical, and are suffused with an isotropic UV field with $G_0 = 1$. The initial density structure of the clouds differed from calculation to calculation. Uniform density clouds were obtained by placing the particles on a body-centered cubic lattice, subject to the condition that they lie within the required spherical volume.

Calculations were also performed for clouds with initial radial density profiles of the form $\rho \propto r^{-s}$, where s takes the values $s = 1/4, 1/2, 1$. In these cases, spherical uniform density clouds of the required masses and radii were used to generate the desired density profiles by applying a stretching transformation to the particle positions, keeping the masses and radii of the clouds the same.

The initial velocities of all particles was set to zero for all of the calculations. Clouds of the required number density n were obtained by fixing the mass and initial radius of the cloud. The initial temperature of all clouds was set at $T = 60$ K, though the thermal time scale is sufficiently short that the clouds develop a thermal structure that is close to that of thermal equilibrium within one time step. When discussing the initial thermal state of a cloud in later sections, we will be referring to the thermal state after a single time step, when a thermal gradient has been established.

The initial conditions adopted for the chemical species are described in the Appendix. In all of the models that we considered, the extinction and density throughout the clouds is sufficiently low that little CO is able to form initially, and carbon is primarily in the form of C^+.

The calculations presented in NL97 were for more massive clouds than those considered here. The outer boundary condition employed in those calculations consisted of a rigid, reflecting surface placed at the original cloud radius, which prevented particles from leaving the computational domain. Test calculations indicated that this boundary condition had little effect on the interior collapsing regions. The calculations presented in this paper are for clouds that are marginally stable/unstable to gravitational collapse, so it is reasonable to assume that the interaction of the clouds with their outer boundary will be more important in determining the outcome of the calculations. In particular, the heating of the surface layers of a cloud will cause these regions to photoevaporate, leading to substantial expansion of the cloud envelope. The rate at which material photoevaporates from the cloud will undoubtedly affect the cloud's gravitational stability, with a higher rate of mass loss making collapse less likely. The use of a constant volume boundary condition holding the cloud material within its original radius thus appears inappropriate in the context of calculations designed to study the gravitational stability of isolated clouds.

It is generally thought that there exists a warm, low density intercloud medium within the Galaxy which is able to provide a confining pressure that will reduce the mass loss rate of photoevaporating clouds. Observations of the outer limbs of molecular clouds indicate the existence of isobaric, atomic halos (Anderson & Wannier 1992) which will similarly regulate the mass loss rates from the underlying clouds. The appropriate boundary condition thus appears to be a constant pressure boundary condition which will allow the cloud envelope to expand, but which will reduce the mass loss rate to a level below that which would occur if the cloud were situated in a vacuum. In order to implement such a boundary condition, we adopt the very simple approach first introduced by Lattanzio *et al.* (1985) and described in Monaghan (1992). The

leading term in the pressure force equation in our formulation of SPH reads:

$$\frac{d\mathbf{v}_i}{dt} = -\sum_{j=1}^{N} m_j \left(\frac{P_i}{\rho_i^2} + \frac{P_j}{\rho_j^2} \right) \nabla_i W_{ij} \tag{9}$$

where W_{ij} is the smoothing kernel and m_j is the particle mass. The constant pressure condition in our calculations is implemented by replacing the $\left(\frac{P_i}{\rho_i^2} + \frac{P_j}{\rho_j^2}\right)$ factor with $\left(\frac{P_i - P_{ext}}{\rho_i^2} + \frac{P_j}{\rho_j^2}\right)$, where P_{ext} is the constant external pressure. This replacement is only introduced during the calculations for those particles whose smoothing lengths overlap an imaginary spherical boundary of fixed radius that coincides with the original surface of the cloud, and for particles that migrate beyond this fixed radius. The external pressure is only included in the summation given in equation (9) when $(r_j < r_i)$, ensuring that the external pressure force is always directed inwards. It should be noted that this procedure is not designed to give a highly accurate description of the interaction between a photoevaporating cloud and an external medium, but rather to provide an inwardly directed pressure force whose characteristic magnitude is similar to that expected from a warm, low density medium. The external pressure that we adopt corresponds to an external medium composed primarily of atomic hydrogen with $n(\mathrm{HI}) = 10$ cm^{-3} and $T \simeq 100$ K.

The majority of the calculations were performed with the constant pressure boundary condition implemented, and with an outflow condition imposed beyond a fixed radius, equal to twice the original radius of the cloud. Material that expanded beyond this radius was simply removed from the calculation. By this time, these particles represent very low density material, and so provide little UV extinction or other influence in the simulations. Calculations were also performed to test the effect of changing the boundary conditions. For example, the external pressure was set to $P_{ext} = 0$, and the outflow condition was removed. These tests are described in subsequent sections.

4. Results

The aim of the work presented here is to examine the gravitational stability of isolated, low mass, interstellar clouds, and to provide a representative collapse calculation including chemical tracers. In particular, we wish to determine how massive a cloud of a particular initial number density needs to be in order for it to undergo collapse, and to understand the physical processes that lead to this collapse. Additionally, we are interested in exploring the form that this collapse takes, and in establishing the density and chemical profiles of collapsing clouds so that they may be compared with observations of isolated Bok globules.

We have examined the gravitational stability of clouds with the following initial number densities: 50, 100, 200, 500, and 1000 cm^{-3}. The results of this numerical stability analysis are presented in Table 1. A description of the contents of each column is given in the caption. A graphical representation of the zones of stability and instability in the mass–density plane is

given in Fig. 1. Clouds that exist above the line drawn in this figure during their earliest stages of evolution should undergo gravitational collapse, whereas clouds that exist below this line are expected to be stable and to eventually photoevaporate. We have found that the main dynamical characteristics of each of the collapse calculations are very similar, and are largely independent of the initial density of the cloud (at least within the range of parameters that we have explored). We have therefore selected one representative example to discuss in detail, which will suffice to illustrate the broad features of the collapse calculations.

4.1. An Illustrative Example of Collapse

We take the $n = 100$ cm^{-3}, $M = 35$ M$_\odot$, $R = 1.2$ pc cloud as our representative case when describing the collapse of isolated clouds. The collapse calculations performed for the clouds whose initial number densities were $n = 50$, 200, 500, and 1000 cm^{-3} were found to be qualitatively similar, and will be discussed briefly at the end of this section.

The time evolution of the density, temperature, radial velocity, and chemical abundance profiles through the cloud are shown in Figs. 2a to 2d. The time, in units of 10^6 yr, corresponding to each of the figures in Fig. 2 is shown at the top right hand corner of the top left hand panel. When describing the individual panels in each figure, we will refer to the top left panel as panel 1, the top right panel as panel 2, the bottom left panel as panel 3, and the remaining panel as panel 4.

The time evolution of α, the ratio of the thermal to gravitational energy in the cloud, is shown in Fig. 3, and illustrates the transition from stability to instability in the inner regions of the cloud as it evolves. Each of the lines drawn in Fig. 3 correspond to estimates of α for different regions of the cloud within different radii. For example, the estimates of α corresponding to $r = 0.1$ in Fig. 3 involved calculating the gravitational and thermal energy of material only within $r = 0.1$ pc at different times during the calculation. This procedure was followed for all values of r shown in Fig. 3. We note that the virial theorem indicates that a cloud becomes gravitationally unstable when $\alpha \simeq 0.5$. The fact that this occurs for $r = 0.1$ and 0.2 pc after $t \simeq 2.7$ Myr indicates that the inner 0.2 pc of the cloud start to undergo gravitational collapse at this time.

Beginning with Fig. 2a, panel 1 shows the density (solid line) and temperature (dotted line) profiles very shortly after the initiation of the calculation ($t = 0.02$ Myr), and panel 2 shows the radial velocity profile, where a negative velocity represents expansion of the material and a positive velocity signifies contraction. Panel 3 shows the fractional abundance profiles of the species C^+, CI, CO, CH_x, and HCO^+, and panel 4 shows the abundance profiles of OI, OH_x, He^+, H_3^+, e^-, and M^+. At this point in time, the density of the cloud is such that the UV extinction and density are low, and CO is unable to form in any meaningful abundance. The temperature and chemical profiles shown correspond to the equilibrium profiles expected for a cloud with the uniform density structure illustrated in panel 1, since the thermal and chemical time scales are

short compared to the dynamical time scale at this point. Inspection of Fig. 3 indicates that the cloud is gravitationally stable against collapse at this point, with $\alpha \sim 6$ for $r = 1$ pc.

When the calculation is initiated, a monotonic temperature and pressure gradient is established through the cloud, with the surface being warmer than the interior. This arises because the UV radiation is preferentially absorbed in the outer layers of the cloud. The resulting inward pushing pressure force drives a pressure wave into the cloud interior, compressing it in the process.

Fig. 2b shows the state of the cloud after it has evolved from its original structure at $t = 1.48$ Myr. The density profile in panel 1 shows the effect of the inward propagating pressure wave. The warm, outer layers of the cloud have expanded outwards, reducing the density in the outer region of the cloud to $n \sim$ few cm^{-3}. The temperature in this region has risen to $T \simeq 200$ K, and shows a turnover in the outermost parts where the density decreases to $n \leq 5$ cm^{-3}. This turnover arises because the dust grains become positively charged at low density when the dust grain–electron recombination rate decreases below the photoejection rate. The increase in grain work function due to the charging of the grains leads to substantial reduction in the photoelectric heating rate, and hence to a reduction in the temperature.

The density in the cloud interior starts to increase as the cloud relaxes in its gravitational potential well, and as it is compressed by the initial pressure gradient. The pressure wave may be observed as a density maximum at a radius of $r \simeq 0.5$ pc. The temperature in the interior has decreased to $T \simeq 25$ K, below its original value of $T \simeq 60$ K, due to the enhanced UV extinction and the increased cooling efficiency at higher density. The increase in density and decrease in temperature causes the values of α plotted in Fig. (3) to decrease as the relative importance of the gravitational forces increases.

Panel 2 shows the radial velocity structure in the cloud. The outer regions are seen to be expanding away from the original cloud surface ($r = 1.2$ pc), since the gas in this region is photoevaporating. The inner regions of the cloud are moving inwards at a velocity of $v_r \simeq 0.2$ km s^{-1} , which is close to the sound speed in a $T \sim 20$ K molecular hydrogen gas. Examination of the evolution of the velocity structure in the cloud up to this point indicates that the motion is induced by the pressure wave and not by gravitational contraction since the cloud is gravitationally stable at this point (*i.e.* $\alpha > 1$ in Fig. 3).

Panels 3 and 4 show the chemical abundance profiles of the cloud. The carbon bearing species can be seen to be evolving, with increases in the abundances of CI and CO relative to C^+ occurring. The profiles of these species correlate with the density since the production rates scale $\propto n^2$ for the formation of CO and CI. The general abundances of these species increases because the increased UV extinction through the cloud reduces the ionization and photodissociation rates. However, the fractional abundances of CO, CH_x and OH_x are low (although the CO and CH_x are at detectable levels), while CI makes up only 1 percent of the carbon.

Fig. 2c shows the state of the cloud after it has evolved for $t = 2.64$ Myr. A similar plot is shown in Fig. 4 for the same moment in time, but with the radius plotted as a linear rather than

logarithmic variable. Panel 1 shows that the peak density has now risen to $n \simeq 2 \times 10^4$ cm^{-3} due to the compression of the cloud. The temperature in the cloud interior has dropped to $T \simeq 8$ K, which is the equilibrium temperature of the shielded regions which are cooled primarily though the line emission of CO and its isotopes and heated by cosmic ray ionization and H_2 formation. The density in the outer layers of the cloud remains low and the temperatures warm. The velocity field in panel 2 of Fig. 2c remains similar to that shown in Fig. 2b, except that the higher velocities are being induced in the material closer to the cloud center as the cloud becomes more compressed. We note that the gravitational forces in the cloud are becoming more influential as the cloud collapses, since the temperature has decreased and the density has increased. Fig. 3 indicates that the value of α in the inner 0.2 – 0.3 pc has dropped to $\alpha \sim 2$ from initially much higher values.

Now that the density in the cloud has increased substantially in the inner regions, there has been a corresponding change in the chemical structure of the cloud, as illustrated by panels 3 and 4 of Fig. 2c. There exists a sharp transition in the primary carbon bearing species, occurring where C^+, CI, and CO are of comparable abundance at a radius of $r \simeq 0.15$ pc. Outside of this radius, the carbon is primarily in C^+. Deep in the interior to this region it is essentially all in the form of CO. Appreciable CI exists primarily in a thin shell surrounding this CO core, dropping off sharply within $r \simeq 0.01$ pc. The CH_x species peak at the previously described transition radius, but even there remain at $X(CH_x) \lesssim 10^{-7}$. The HCO^+ shows a substantial rise in the cloud interior, peaking at around $X(HCO^+) \simeq 5 \times 10^{-9}$. The conversion of C^+ and CI to CO in the cloud interior leads to a drop in OI from $X(OI) = 2 \times 10^{-4}$ in the envelope to 1×10^{-4} in the interior. The abundance of the OH_x species rises to about $X(OH_x) \simeq 7 \times 10^{-6}$ in the shielded interior since it is no longer photodissociated.

The structure of the cloud after evolving for $t = 3.34$ Myr is shown in Fig. 2d. Panel 1 shows that the density has increased at the cloud center to $n \sim 10^7$ cm^{-3}. The temperature in these dense inner regions is $T = 10$ K, since the gas–dust thermal coupling now dominates the thermal evolution of the gas at these high densities. Material with densities of $n \sim 10^4$ to 10^5 cm^{-3} in the inner shielded region has a temperature $T \simeq 8$ K. For material with densities $n \gtrsim 10^5$ cm^{-3}, there is a slight rise in temperature to $T \sim 12$ K because the compressional PdV work term contributes to the heating as these regions of the cloud start to undergo gravitational collapse. For material with densities $n \gtrsim 10^6$ cm^{-3}, the dust cooling dominates and the gas is held fixed at $T = 10$ K. The plots of α versus time for different radii shown in Fig. 3 indicate that gravitational instability has occurred in the central ~ 0.1 – 0.2 pc of the cloud. The radial velocity profile shown in panel 2 of Fig. 2d shows a change from earlier times, with higher velocities beginning to develop within $r \sim 0.1$ pc, and a double humped structure occurring. This feature arises from the gravitational instability of the inner region, leading to the growth of large velocities there. The velocity profile at later times than those displayed in Fig. 2d shows that the whole of the inner region within $r \lesssim 0.1$ pc eventually develops large velocities as the gravitational collapse continues to higher densities beyond $n = 10^7$ cm^{-3}. We are primarily interested in modeling the evolution of the clouds up to their initial collapse phase, and do not show the results for times beyond this point.

The chemical abundance profiles corresponding to this point in time, when the inner region of the cloud has just become gravitationally unstable, are shown in panels 3 and 4. They differ only slightly from the profiles shown in Fig. 2c ($t = 2.64$ Myr), since most of the chemical evolution takes place by the time the peak density reaches $n \sim 10^5$ cm^{-3}. We note that the CI abundance drops dramatically in the very center of the cloud, as it converts to CO. The OH_x species has continued to increase its abundance, and has risen to $X(OH_x) \simeq 10^{-5}$ in the interior. For densities beyond 10^{5-6} cm^{-3} depletion onto cold dust grains is important for polar molecules such as OH and H_2O and even CO for sufficiently cold dust (cf. Bergin *et al.* 1995, Bergin & Langer 1997). As we do not include depletion and desorption mechanisms, the gas phase chemical abundances could be an overestimate in the innermost 0.01 pc at such late times.

In summary, the cloud has evolved from a diffuse, uniform density object to one that has a distinctive core–halo structure. The core consists of cold, dense gas in which there is a high abundance of CO and the OH_x species, whereas the halo contains warm, diffuse gas in which the trace species of C and O are primarily in ionic (C^+) and atomic (OI) form. The original cloud was gravitationally stable, but evolved to a state of gravitational instability through a combination of dynamical, thermal, and chemical evolution. This calculation illustrates the possible importance of pressure forces acting in an isolated, externally heated cloud in shaping its long term evolution.

4.2. Salient Features of the Collapse Solutions

4.2.1. Density Profiles

A number of similarities exist in the collapse solutions obtained for clouds of differing initial number density. In particular, the radial density profiles obtained in each case appear to be almost indistinguishable from one another, with each calculation producing the near power law profiles shown in Figs. 2c and 2d. We have established that the density profile through the cloud at the earlier stage of evolution (Fig. 2c), prior to the formation of a dense core region and gravitational collapse, may be approximated by the form $\rho \propto r^{-2}$. The density profile in the inner 0.1 pc measured at a time that corresponds to Fig. 2d is found to steepen once collapse starts to occur, and may instead be approximated by the power law $\rho \propto r^{-2.5}$. This is somewhat steeper than the similarity solution for a collapsing, isothermal sphere which usually takes the form $n \propto r^{-2}$ (e.g. Larson 1969). We have performed a number of collapse calculations for isothermal spheres containing various numbers of Jeans masses, and find that the similarity solution does not hold exactly for these calculations either, and that steeper profiles do indeed occur with values of the power law exponent being typically $s \sim 2.5$. The central regions of our clouds are very nearly isothermal when they eventually start to collapse, with $T \simeq 10$ K, and appear to generate collapse profiles similar to the isothermal ones. The effects of the warm, low density envelope and the earlier evolution of the cloud do not appear to affect the collapse profiles substantially. We remark that similar density profiles have been reported to exist in starless Bok globules by Kane

& Clemens (1997).

4.2.2. Velocity Profiles

The velocity structure generated in the clouds during the early epochs of their evolution arises primarily because of the external heating, and the action of the resulting inward pushing pressure gradient. The outer parts of the cloud show strong outward motion as the surface layers are photoevaporated. The region just below the surface is accelerated inwards by the higher pressure exterior, up to velocities of $\simeq 0.2$ km s^{-1}, and the deep interior remains relatively quiescent until later times.

As the evolution continues, the velocity profile in the outer parts remains relatively unchanged, whereas it changes substantially in the interior. The continued propagation of the pressure wave into the cloud excites inward motion there, because the cloud is being compressed. As the cloud evolves towards gravitational instability and collapse, the dense inner regions develop large inward velocities which quickly exceed the local sound speed as the collapse gets underway. The velocity profile in the collapsing core is similar to that which arises during the collapse of an isothermal sphere, since the core is in fact isothermal when collapse is initiated.

The envelope of material, with density $n \simeq 10^4 - 10^5$ cm^{-3}, which surrounds the collapsing core also shows inward velocities which is remnant motion arising from the initial pressure gradient that existed through the cloud, and not from gravitational collapse, and so is indicative of the early evolution of the cloud prior to collapse ensuing. Thus, observations which indicate either a quiescent core surrounded by an envelope with larger line widths, or a collapsing core surrounded by an envelope with $n \sim 10^4$ cm^{-3} which also showed a signature of substantial inward motions, could be interpreted as arising from cloud evolution that was in part initiated by the existence of a pressure gradient arising from the external UV field. We note, however, that these motions will not result in substantial line broadening since the inward velocities $\simeq c_s$, the local sound speed.

4.2.3. Dense Core Masses

We typically stopped running the calculations shortly after gravitational collapse started to occur in the dense cores, when the peak density was $n \simeq 10^7$ cm^{-3}. We define a dense core to consist of material that has a fractional CO abundance of $X(\mathrm{CO}) \geq 10^{-6}$, since this is close to the detection limit of ^{12}CO in Bok globules in observational surveys using single dish radio telescopes such as those performed by Clemens & Barvainis (1988) and Clemens, Yun, & Heyer (1991). We have measured the amount of mass with $X(^{12}\mathrm{CO}) \geq 10^{-6}$ in the cores generated by our simulations. Typically, about 20 to 25 per cent of the original cloud mass is contained in the cores at the point at which they are stopped. In the case of the $n = 100$ cm^{-3}, $M = 35$ M$_\odot$, $R = 1.2$ pc cloud, this amounts to $M_{core} \sim 7\mathrm{M}_\odot$. For the initially higher density cloud of $n = 1000$ cm^{-3},

$M = 10$ $M_\odot$, and $R = 0.36$ pc, the core mass is estimated to be $M_{core} \sim 2.5$ $M_\odot$ at the point when the peak density reaches $\sim 10^7 cm^{-3}$.

We note that the velocity structure in the cloud is such that material which is outside of the dense, collapsing core still possesses large inward velocities, arising from the initial compression of the cloud by the pressure gradient caused by externally heating the cloud. If the calculations were continued beyond the point where the density rises above $n \sim 10^7$ cm^{-3}, then it is expected that the core mass will continue to grow substantially beyond our current estimates. We also note, however, that the dynamical time in the densest regions of the cloud becomes shorter as the density increases, and that in a realistic situation a protostar with an accompanying wind/outflow is likely to form before this infalling envelope of material has had an opportunity to accrete onto the dense core. We are thus unable to estimate the final mass of any dense core/protostar that might be expected to arise from these calculations, but we are able to estimate the mass of the dense core in its earlier stages of collapse, and do not expect it to change substantially during the subsequent evolution.

4.3. Effect of Changing Initial Density Profiles

The majority of the calculations that we have performed assumed that the clouds were of uniform density to start with. The fact that the clouds were initially gravitationally stable, with $\alpha \sim 5 - 6$, means that large degrees of central condensation should not be expected. In order to examine the effect of deviating from this assumption, a number of calculations were performed with initial density profiles of the form $n(r) \propto r^{-s}$, with s taking the values 1/4, 1/2, and 1. The initial conditions of these simulations are described in section (3).

The results of these calculations indicate that the assumed initial density profile has little effect on the outcome, provided that the cloud is not on the cusp between gravitational stability and instability. For example, calculations were performed with $M = 35$ $M_\odot$ and $R = 1.2$ pc. We note that a uniform density cloud with these parameters had a mean number density of $\bar{n} = 100$ cm^{-3}, and was found to be gravitationally unstable. Reducing the mass slightly to $M = 30$ $M_\odot$, but maintaining a uniform density of $n = 100$ cm^{-3}, yields a cloud model which is gravitationally stable (see table [1]), indicating that the $M = 35$ $M_\odot$ is only marginally unstable. The centrally condensed cloud models with $M = 35$ $M_\odot$ and $R = 1.2$ pc were found to be gravitationally stable if $s = 1/2$ or 1, but gravitationally unstable if $s = 1/4$. If the mass were increased to $M = 40$ $M_\odot$ and radius to $R = 1.25$ pc, keeping the mean number density $\bar{n} = 100$ cm^{-3}, then all the calculations (with $s = 1/4$, 1/2, and 1) resulted in gravitational collapse. The reason for this behavior is that the clouds all start off gravitationally stable. Now that the density profile is no longer uniform, the external heating provides a temperature through the cloud that increases with radius from the center, but the pressure is found to decrease with radius, such that the central regions of the cloud wish to re–expand, and are not under the influence of a higher pressure envelope. The expansion of the central parts of the cloud causes it to evolve towards a quasi uniform density structure, such

that the temperature and pressure profiles change, and the pressure becomes higher at the outer parts of the cloud than the inner parts. The situation is now similar to that which exists at the beginning of the calculations of evolving, uniform density clouds described in section (4.1), with the difference being that the cloud material has acquired some outwardly directed momentum due to its initial expansion. The question of whether such a cloud can collapse is determined by the ability of the inwardly directed pressure force to overcome this outward momentum, and to recompress the inner part of the cloud to a point where it becomes gravitationally unstable. We find that the clouds which are only marginally unstable to gravitational collapse, when they start off as uniform objects, may be rendered gravitationally stable by starting off with substantial central condensation (*i.e.* $s = 1/2$ or 1), but still collapse with mild initial central condensation ($s = 1/4$). Clouds which are slightly more massive than these marginal cases are able to collapse irrespective of their initial density profiles.

The evolution of the $M = 40$ $M_\odot$, $R = 1.25$ pc, $s = 1$ cloud model is shown in Figs. 5a–c. Panel 1 of this figure shows the initial density (solid line) and temperature (dotted line) profiles, panel 2 shows the radial velocity, and panels 3 and 4 show the fractional abundances of the chemical species included in the model. The density profile shown in panel 1 indicates that the cloud is initially quite centrally condensed, with a peak number density of $n \simeq 3000$ cm^{-3}. The temperature shows an inverse profile relative to the density, as expected, with a central temperature of $T \simeq 20$ K and a surface temperature of $T \simeq 80$ K. The chemical abundance profiles plotted in panels 3 and 4 indicate that the extra UV extinction through the cloud, caused by its density profile, allows the molecular species CO and OH_x to exist in greater abundance initially than if the cloud were initially uniform, as illustrated in Fig. 2a.

As the calculation proceeds, the central density decreases as the inner regions of the cloud expand, since the cloud is strongly stable against gravitational collapse in its current state. As the density profile evolves towards being approximately uniform, the pressure profile through the cloud evolves until the direction of the pressure gradient is reversed, and the cloud interior feels an inward push rather than one which causes it to expand. This is illustrated in panel 1 of Fig. 5b, where the inward moving pressure wave may be observed as a density maximum located at $r \simeq 0.3$ pc. The temperature profile is now very similar to that observed in Fig. 2b. In addition, the velocity field plotted in panel 2 shows the development of inwardly directed motion, after the initial expansion of the cloud, as a result of the inwardly directed pressure force. The expansion of the cloud center has lowered the UV extinction there, and as a consequence the abundance of molecules (e.g. CO) has diminished due to the enhanced dissociation. The subsequent evolution of the cloud is almost identical to that described for the initially uniform density cloud in section (4.1). Comparison between Figs. 2d and 5c shows that the thermal, density, chemical, and kinematic structure of the clouds at the end of the calculations are almost identical, and are not substantially affected by the assumed initial conditions.

4.4. Effects of Changing Boundary Conditions

As described in section (3), we have run a number of test cases to examine the effects of changing the outer boundary conditions. Our motivation for performing these tests is the recognition that the gravitational stability of an externally heated, isolated molecular cloud may in part be determined by the rate at which material is able to photoevaporate from the cloud surface. If material is able to photoevaporate more rapidly as the underlying cloud evolves, one might suppose that the cloud is less likely to undergo collapse than if this photoevaporation were inhibited.

The boundary condition that we have employed consists of a constant pressure boundary condition, which retards the rate at which a cloud may expand, and an outflow condition that allows material to leave the system after it has expanded beyond a given, fixed radius (usually equal to twice the original radius of the cloud). We have performed a number of calculations to test the effect of changing the radius at which the outflow condition is invoked, and have found that moving it out from twice the initial cloud radius to three times the initial radius makes no qualitative difference to the results. We therefore conclude that the application of an outflow condition plays little role in determining the outcome of the calculations.

We have also run test calculations to examine the effects of changing the constant pressure condition. In these calculations we removed the external pressure completely so that the clouds were able to freely expand out into a vacuum. In the case of the clouds which start with $n = 100$ cm^{-3}, we found that the criterion for collapse was altered by this change in external pressure. With a finite P_{ext} we found that the cross over between stability and instability occurred for clouds with masses between 30 and 35 $M_{\odot}$. If we set $P_{ext} = 0$, then this cross over in mass instead occurred between 35 and 40 $M_{\odot}$. We interpret this to mean that the gravitational stability of an externally heated, isolated cloud is in part determined by the rate at which material is able to photoevaporate from the cloud surface. We emphasize that the external pressure that we include as our boundary condition is not itself responsible for driving the collapse of the clouds, because the internal pressures of the clouds are higher than the external pressure that we employ in all cases. The external pressure that we have employed is a reasonable estimate of what is to be expected for a warm, low density intercloud medium, so that the masses that we have obtained in our numerical stability analysis of collapsing clouds are probably good estimates of the region of cross over from stability to instability for isolated, low mass, thermally supported clouds.

5. Discussion

In the previous sections, we have presented the results from a series of numerical simulations that follow the combined thermal, chemical, and dynamical evolution of low mass molecular clouds from an initially diffuse state. The primary purpose of these simulations was to determine the effective 'Jeans mass' of such objects, which are heated externally by the ISRF, as a function of

their initial number density. The neglect of turbulent motions and magnetic fields, which provide additional support against gravitational collapse, means that these numerically determined 'Jeans masses' should be interpreted as being lower limits.

5.1. Comparison with Observations

A number of observational studies of isolated, low mass molecular clouds (Bok globules) have appeared in the literature. A catalogue of 248 of these objects was compiled by Clemens & Barvainis (1988) from the POSS plates. Clemens *et al.* (1991) detected 244 of these in the CO ($J = 2 \rightarrow 1$) transition. Many of the objects have been shown to have infrared colors consistent with Class I sources (Yun & Clemens 1994a), and some contain radio sources with no infrared counterparts (Yun *et al.* 1996), which is the predicted signature of Class 0 protostars. Furthermore, a number of globules have outflows (Yun & Clemens 1994b, Henning & Launhardt 1998), which is a sign of on–going star formation. According to the currently accepted paradigm of star formation, stars form *via* the collapse of dense, molecular cloud cores, so that a prerequisite for star formation is the existence of dense gas. A number of millimetre studies have appeared in the literature using the tracers of dense gas such as ammonia (NH_3) and CS (Bourke *et al.* 1995, Henning & Launhardt 1998, Launhardt *et al.* 1998). These studies indicate a strong correlation between the detection of line emission from these tracers and other signatures of dense gas such as millimetre continuum emission, and the detection of $C^{18}O$ (Henning & Launhardt 1998). In addition, these signatures are found to occur ubiquitously in cloud cores that show signs of containing either Class I or Class 0 protostars, suggesting that these objects are in the process of forming stars by accreting from the dense, gaseous envelopes in which they are embedded. Many of the studies of Bok globules contain biases in their selection criteria that preferentially pick out globules that show signs of star formation. There exists, however, a class of globule which show no obvious signs of star formation (the so–called 'starless globules'). Nonetheless, the existence of dense gas in some of these globules ($\sim$ 40 per cent – Launhardt *et al.* 1998), suggests that they may be in a pre protostellar stage.

The estimated mass of the lower mass examples of these objects are typically in the range 0.2 – 35 $M_\odot$ (e.g. Launhardt *et al.* 1997), with the higher mass globules showing signs of small cluster formation (Yun & Clemens 1994a, Alvez & Yun 1995), and the lower masses being either starless, or being the sites of single or binary star formation. The derived masses of these lower mass globules compare favorably with the 'Jeans mass' estimates that come out of our simulations, when we account for the percentage of cloud material that becomes incorporated within the dense molecular core. This fraction is typically 20 – 30 per cent, which leads to core masses of between 3 – 20 $M_\odot$. Observed globule cores that are substantially more massive than this, but contain no protostars, are presumably evolving towards collapse, or are being prevented from a further increase in density by the presence of turbulence or magnetic fields. In this case, star formation will have to await the decay of this turbulence, or will be prevented by the gradual erosion of the

cloud through its evaporation by the ISRF. We remark that the observed sizes of the dense cores in Bok globules are typically $r \sim 0.1 - 0.3$ pc. The sizes of the dense cores that are formed in the simulations fall precisely in this range.

In addition to measuring the masses and radii of the globules, the observational surveys have also measured the gas and dust temperatures in the dense cores. The gas temperature is typically measured to be ~ 10 K, which is very consistent with our simulations which predict temperatures between 8 – 12 K in regions where $10^4 \lesssim n \lesssim 10^7$ cm^{-3}. The dust temperatures are measured to be rather higher ($T_d \sim 20$ K), which may be accounted for by the existence of a temperature gradient in the globules, or by the existence of small, transiently heated grains, since the dense gas should be thermally coupled to the dust for $n > 10^5 - 10^6$ cm^{-3}. Our calculations in essence assume a fixed dust temperature, and so cannot yet be compared with observations.

There have been few measurements of the density profiles in Bok globules that we can compare with our numerical simulations. The object B335 has been investigated by many authors, and has been shown to exhibit the features expected from an isothermal collapse (e.g. Zhou *et al.* 1993, 1994. See also Chandler & Sergeant 1993, Velusamy *et al.* 1995). Our calculations indicate that gravitational collapse only occurs in a cloud that is evolving from an initially low density state when a dense, cold, isothermal core has been formed at its center, such that the collapsing dense cores of Bok globules should indeed look like collapsing isothermal clouds. The fact that the globule has undergone a period of prior evolution that was not isothermal does not seem to affect the form of the collapse of the isothermal core. Yun & Clemens (1991) have examined the density structure of a number of globules containing YSO candidates, and derived density profiles of $\rho \propto r^{-1.6}$. More recently, Kane & Clemens (1997) have reported the measurement of density profiles in 'starless globules' which appear to have steeper profiles corresponding to $\rho \propto r^{-2.6}$. Our simulations produce similar density profiles to these. During the early stages of evolution, prior to the formation and collapse of a dense core, when the maximum number density is $n_{max} \sim 10^4$ cm^{-3}, a density profile corresponding to $\rho \propto r^{-2}$ is etsablished throughout the cloud. When a collapsing, dense core has been formed, the profile appears to steepen, resulting in $\rho \propto r^{-2.5}$. This suggests that the globules reported by Kane & Clemens (1997) may be evolving towards gravitational collapse, and the formation of stars.

5.2. Formation of Bok Globules

Superficially, Bok globules appear to be low mass molecular clouds that are isolated from any other regions of star formation. Recent work by Henning & Launhardt (1997), however, indicates that many of the globules are in fact loosely associated with larger star forming complexes. This association suggests that the globules are remnants of these larger complexes that were left exposed when the lower density material of the cloud complex was blown away by some process, such as a supernova, or through photoevaporation. An alternative formation mechanism is the possibility that the globules were formed *in situ* through the contraction of truly isolated, and

initially diffuse material.

The calculations presented in earlier sections cover a broad span in the initial number density, and so can be applied to both of these formation mechanisms. The lower density clouds illustrate the evolution of an isolated globule from an initially diffuse state, towards a higher density object, and show how an initially isolated, low density cloud could evolve to form a dense molecular core and protostar. The clouds which start from higher densities (e.g. 1000 cm^{-3}), can be imagined to have been higher density components of a larger complex, which shielded it from the ISRF, and became isolated when this shielding medium was dispersed. These simulations are therefore more appropriate to the Bok globule formation mechanism of Henning & Launhardt (1997). The similarity in the results of the simulations indicate that the actual formation mechanisms of Bok globules may not play a major role in determining the details of their long term evolution.

6. Conclusions

The main conclusions to be drawn from the calculations presented in this paper are as follows:

(1). Initially diffuse, and gravitationally stable clouds may evolve towards denser objects which undergo gravitational collapse.

(2). The evolution of these isolated, thermally supported, objects is driven initially by a temperature and pressure gradient through the cloud which is created by the attenuation of the FUV component of the ISRF.

(3). As the clouds evolve, they undergo significant thermal and chemical evolution. The end result is a core–halo structure, where a cold, dense core, in which the trace species are bound up in molecules (e.g. CO), is surrounded by a warm, diffuse envelope, where the carbon is in ionic form (CII), and the molecules of the trace species are dissociated.

(4). Effective 'Jeans masses' as functions of the initial number density were obtained. Initially diffuse clouds (n = 50 – 100 cm^{-3}) need to contain at least 35 – 60 $M_{\odot}$ of material before they can collapse. Denser clouds (e.g. n = 1000 cm^{-3}) require $\sim$ 10 $M_{\odot}$ before they can collapse.

(5). The dense molecular cores that develop in the simulations typically contain 20 – 30 per cent of the original cloud. The rest forms an envelope around the core, and is steadily photoevaporated by the ISRF. This result indicates that only a relatively small fraction of the material in a Bok globule is detectable by observational surveys using molecular tracers.

(6). The gravitational collapse of the core shows the characteristics of a collapsing isothermal sphere, since it evolves towards such an object before gravitational collapse ensues.

(7). The density profiles that arise in the clouds during the simulations are $\rho \propto r^{-2}$ during the initial stages, prior to core formation and collapse, and $\rho \propto r^{-2.5}$ after the collapse of the dense core commences.

The simulations presented in this paper represent an early stage in our attempt to calculate detailed models of the interstellar medium. Further studies are being undertaken to examine the impact of changing the ISRF, and of including the effects of magnetic fields and turbulence on the outcome of the calculations. In addition, we are working on an improved model for calculating the dust temperature.

This research was supported by PPARC rolling theory grant .... This research was conducted at the Jet Propulsion Laboratory, California Institute of Technology under support from the National Aeronautics and Space Administration. We would like to thank Dr. Ted Bergin for useful conversations regarding the calculation of the chemical abundances and the use of LSODE.

REFERENCES

Andersson, B-G., Wannier, P. W. 1992, ApJ, 260, 355

Bergin, E.A., Langer, W.D., 1997, ApJ486, 316

Bergin, E.A., Langer, W.D., Goldsmith, P.F., 1995, ApJ, 441, 222

Bourke, T.L., Hyland, A.R., Robinson, G., 1995a, MNRAS, 276, 1052

Bourke, T.L., Hyland, A.R., Robinson, G., James, S.D., Wright, C.M., 1995b, MNRAS, 276, 1067

Chandler, C.J., Sargeant, A.I., 1993, ApJ, 414, L29

Clemens, D.P., Barvainis, R. 1988, ApJS, 68, 257

Clemens, D.P., Yun, J.L., Heyer, M.H., 1991, ApJS, 75, 877

Genzel, R., 1991, in Proc. of the Conference on Physics ofStar Formation and Early Stellar Evolution, eds. C.J. Lada & N. Kylafis, (Dordrecht: Kluwer Academic), p. 155

Gingold, R.A., Monaghan, J.J., 1977, MNRAS, 181, 375

Goldsmith, P. F., Langer, W.D., 1978, ApJ, 222, 881

Habing, H. 1968, *Bull. Astron. Inst. Neth.*, 19, 421

Henning, Th., Launhardt, R., 1998, Preprint

Hollenbach, D., Tielens, A. G. G. M., Takahashi, T., 1991, ApJ, 377, 192

Kane, B.D, Clemens, D.P., BAAS, 191

Langer, W. D., 1976, ApJ, 206, 699

Larson, R. B. 1969, MNRAS, 145, 271

Launhardt, R., D, Henning, Th., 1997, å, 326, 329

Launhardt, R., Ward–Thompson, D, Henning, Th., 1997, MNRAS, 288, L45

Launhardt, R., Evans, N.J. II, Wang, Y., Clemens, D.P., Henning, Th., Yun, J.L, 1998, Preprint

Lucy, L., 1977, AJ, 83, 1013

Nelson, R.P., Langer, W.D., ApJ, 1997, 482, 796

Nelson, R.P., Papaloizou, J. C. B., 1994, MNRAS, 270, 1

Shematovich, V. I., Shustov, B. M., Wiebe, D. S., 1997, MNRAS, 292, 601

Van Dishoeck, E.F., Black, J.H., 1988, ApJ, 334, 771

Velusamy, T., Kuiper, T.B.H., Langer, W.D., 1995, ApJ, 451, L75

Yun, J.L., Clemens, D.P, 1994a, AJ, 108, 612

Yun, J.L., Clemens, D.P, 1994b, ApJS, 92, 145

Yun, J.L., Moreira, M.C., Torrelles, J.M., Alfonso, J.M., Santos, N.C., 1996, AJ, 111, 841

Zhou, S, Evans, N.J., II, Kompe, C., Walmsley, C.M., 1993, ApJ, 404, 232

Zhou, S, Evans, N.J., II, Kompe, C., Walmsley, C.M., 1994, ApJ, 421, 854

Table 1. Results of Calculations

$n(H_2)$ cm^{-3}	M ($M_\odot$)	R (pc)	Collapse ?
50	60	1.80	Yes
50	50	1.69	No
100	35	1.19	Yes
100	30	1.13	No
200	20	0.78	Yes
200	15	0.71	No
500	15	0.53	Yes
500	10	0.46	No
1000	10	0.36	Yes
1000	8	0.34	No

Note. — First column gives the initial number density, second column gives the cloud mass, third column gives the initial cloud radius, and the fourth column indicates whether the cloud underwent gravitational collapse.

A. Chemical model

The chemical model used here is designed to capture the essentials of the carbon and oxygen chemistry and keep track of the atoms, ions, and molecules responsible for the majority of the cooling in low mass clouds. It is based on constructing a pseudo-reaction set in which only key intermediate reactions are kept which play a role in the conversion of carbon and oxygen among the major gas phase reservoirs (outlined in Langer (1976) and Graedel et al. (1982)). For example, a key reaction to convert carbon ions into molecules in photon dominated regions is, $C^+ + H_2 \rightarrow CH_2^+ + h\nu$, which is rapidly followed by, $CH_2^+ + H_2 \rightarrow CH_3^+ + H$. The molecular ion CH_3^+ reacts rapidly with electrons to dissociate into CH and CH_2. Rather than follow all of these reaction channels, most of which are very rapid compared to the first step, we approximate the reaction as going immediately to its final product, $C^+ + H_2 \rightarrow CH_x + H$, where $CH_x = CH + CH_2$. Comparison of such models to complete reaction sets shows that they are capable of representing very well the transformation of atoms and ions into molecules (cf. Bergin et al. 1995; Shematovich et al. 1997). The chemical reactions that we evolve and their associated reaction rates are given in Table 1. In the present version of the chemistry we have included the effects of self-shielding using the program of Bergin et al. (1995) which is based on the radiative transfer modeling of Black and van Dishoeck (198?). The conservation conditions, total gas phase fractional abundances, and initial conditions are listed in Table 2.

Table 2. Chemical Reaction and Rate Coefficient

Reaction	Reaction Rate Coefficients[a]	Number[b]
Cosmic ray ionization		
$cr + H_2 \rightarrow H_3^+ + e + H + cr$	1.2×10^{-17}	k_1
$cr + He \rightarrow He^+ + e + cr$	6.8×10^{-18}	k_2
Ion–molecule reactions		
$H_3^+ + CI \rightarrow CH_x + H_2$	2×10^{-9}	
$H_3^+ + OI \rightarrow OH_x + H_2$	8×10^{-10}	k_{11}
$H_3^+ + CO \rightarrow HCO^+ + H_2$	1.7×10^{-9}	
$He^+ + H_2 \rightarrow He + H + H^+$	7×10^{-15}	k^{13}
$He^+ + CO \rightarrow C^+ + O + He$	1.6×10^{-9}	
$C^+ + H_2 \rightarrow CH_x + H$	4×10^{-16}	
$C^+ + OH_x \rightarrow HCO^+$	1×10^{-9}	
Neutral–neutral reactions		
$OI + CH_x \rightarrow CO + H$	2×10^{-10}	
$CI + OH_x \rightarrow CO + H$	$5.8 \times 10^{-12} T^{0.5}$	
Electron recombination		
$He^+ + e \rightarrow He + h\nu$	$9 \times 10^{-11} T^{-0.64}$	k_{200}
$H_3^+ + e \rightarrow H + H_2$	$1.9 \times 10^{-6} T^{-0.54}$	k_{201}
$C^+ + e \rightarrow CI + h\nu$	$1.4 \times 10^{-10} T^{-0.61}$	
$HCO^+ + e \rightarrow CO + H$	$3.3 \times 10^{-5} T^{-1.0}$	
$M^+ + e \rightarrow M + h\nu$	$3.8 \times 10^{-10} T^{-0.65}$	
Charge transfer reactions		
$H_3^+ + M \rightarrow M^+ + e + H_2$	2×10^{-9}	
Photoreactions		
$h\nu + CI \rightarrow C^+ + e$	$3 \times 10^{-10} G_0 e^{-3A_v}$	
$h\nu + CH_x \rightarrow CI + H$	$1 \times 10^{-9} G_0 e^{-1.5A_v}$	
$h\nu + CO \rightarrow CI + O$	$10^{-10} \mathcal{S}^c(N(CO), N(H_2)) G_0 e^{-3A_v}$	
$h\nu + OH_x \rightarrow OI + H$	$5 \times 10^{-10} G_0 e^{-1.7A_v}$	
$h\nu + M \rightarrow M^+ + e$	$2 \times 10^{-10} G_0 e^{-1.9A_v}$	
$h\nu + HCO^+ \rightarrow CO + H$	$1.5 \times 10^{-10} G_0 e^{-2.5A_v}$	

[a]The rate coefficients are taken from the UMIST catalog (cf. Bergin et. al. and references therein). Two body reactions are in units of $cm^3\ s^{-1}\ mol^{-1}$, while photoreactions and cosmic ray reactions are in units of $s^{-1}\ mol^{-1}$

[b]Numbers for reactions are noted in the few cases where we use these to define equations for initial conditions in Table 2.

[c]$\mathcal{S}(N(CO), N(H_2))$ is the ^{12}CO self-shielding factor of van Dishoeck & Black (1988) taken from Bergin et al. (1995).

Table 3. Chemical Model Conditions

Reaction
Conservation conditions
$n(e) = n(C^+) + n(He^+) + n(H_3^+) = n(M^+)$
$n(He_{total}) = n(He) + n(He^+)$
$n(M_{total}) = n(M^+) + n(M)$
Initial Fractional Abundances
$n(C_{total}) = 10^{-4} n(H_2)$
$n(O_{total}) = 2 \times 10^{-4} n(H_2)$
$n(He_{total}) = 0.28 n(H_2)$
$n(M_{total}) = 10^{-7} n(H_2)$
Initial conditions
$n(CI) = n(CO) = n(CH_x) = n(HCO^+) = 0$
$n(C^+) = n(C_{total})$
$n(OI) = n(O_{total})$
$n(M^+) = n(M_{total})$
$n(He^+) = \frac{k_2}{k_{200} n(e) + k_{13} n(H_2)} n(He_{total})$
$n(H_3^+) = \frac{k_1}{k_{201} n(e) + k_{11} n(OI)} n(H_2)$
$n(e) = n(C^+) + n(He^+) + n(M^+)$

Fig. 1.— A graphical representation of the zones of stability and instability as a function of the initial cloud mass and number density.

Fig. 2.— This figure shows the time evolution of the number density (solid line), temperature (dotted line), radial velocity, and chemical abundance profiles for the cloud with $M = 35$ $M_\odot$, $R = 1.2$ pc, and an initially uniform density profile with $n = 100$ cm^{-3}. Each plot (2a–d) shows the state of the cloud at different times during the calculation, given in units of Myr at the top right of each top left panel.

Fig. 3.— This figure shows the time evolution of α evaluated within different radii, r, in the cloud. Each line in the plot shows the time evolution of α within a fixed radius. Note that as the cloud evolves, the inner parts of the cloud tend towards gravitational instability such that $\alpha \lesssim 0.5$ for $r \lesssim 0.2$ pc at later times.

Fig. 4.— This figure is the same as Fig 2c, except that it is plotted on a log–linear scale, and shows a snap shot of the density (solid line) and temperature (dotted line) profiles, the radial velocity profile, and the fractional abundances of the various chemical species which are marked on the figure. The cloud started off with $M = 35$ $M_\odot$, $R = 1.2$ pc, and an initially uniform density profile with $n = 100$ cm^{-3}.

Fig. 5.— This figure is similar to Fig. 2, except that it shows the time evolution of the number density, temperature, radial velocity, and chemical abundance profiles for a cloud with $M = 40$ $M_\odot$, $R = 1.25$ pc, and an initial density profile $n \propto r^{-1}$. Comparsion between this figure and Fig. 2, particularly between Fig. 2d and Fig. 5c, shows that the initial density profile has little effect on the final results of the calculation.

Fig. 1 – Mass v's $n(H_2)$ indicating regions of stability

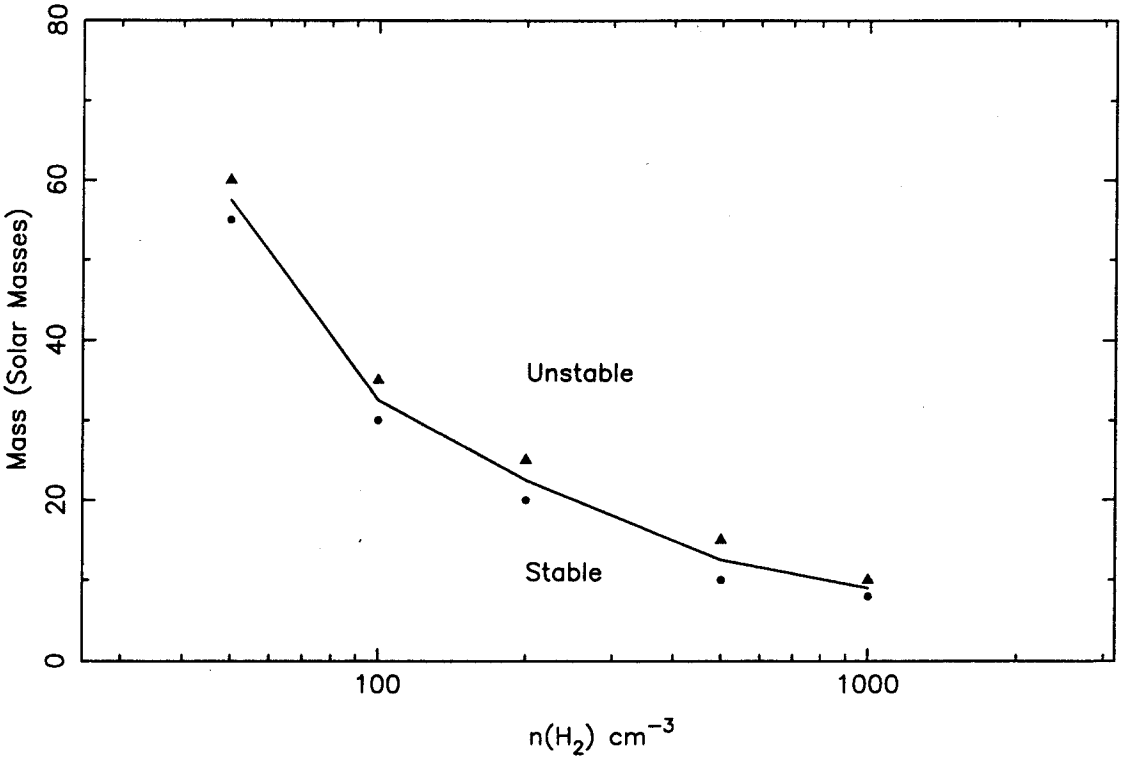

Fig. 2a – n(H2) and T v's r: M=35, R=1.2, n=100

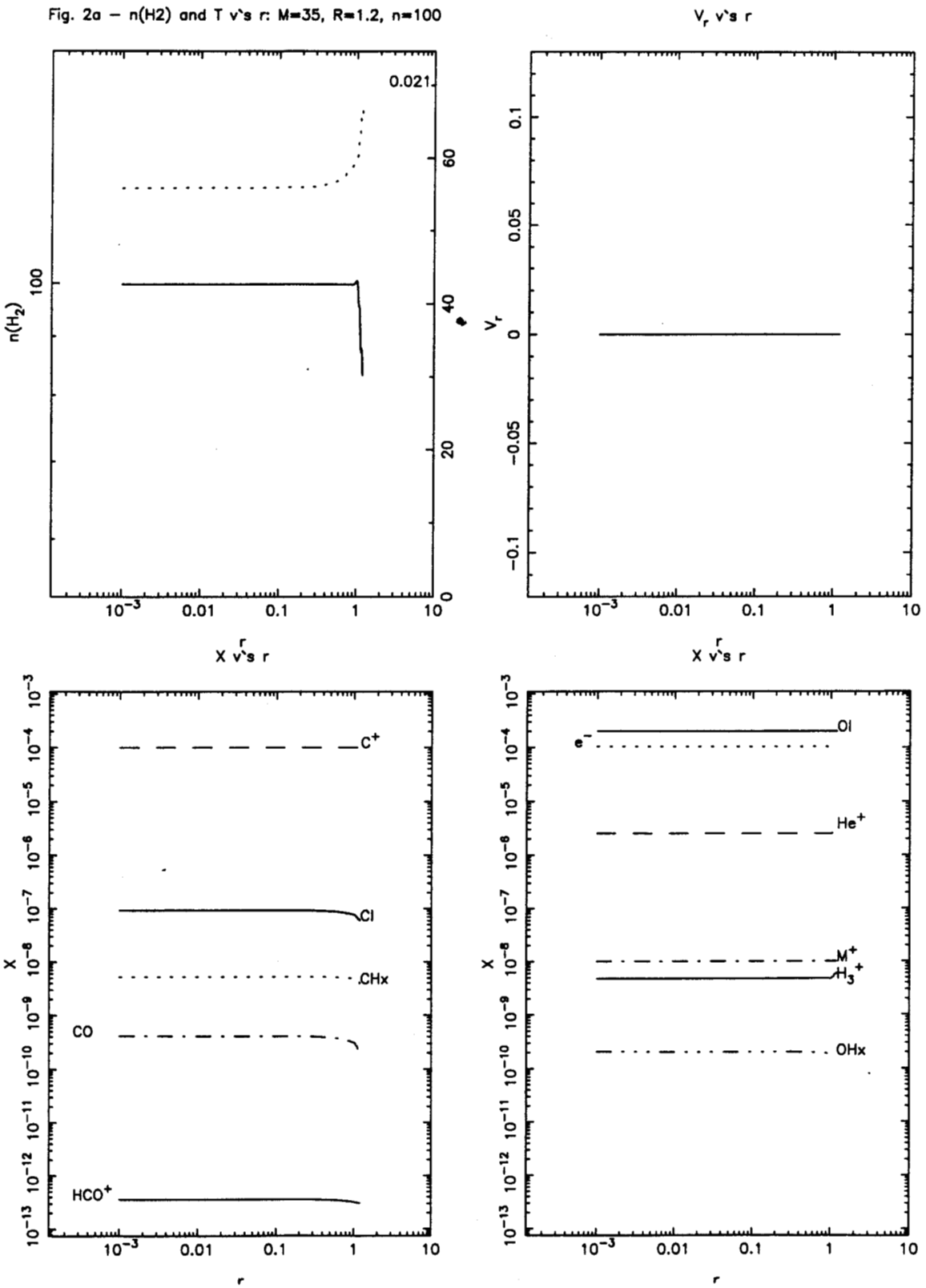

Fig. 2b – n(H2) and T v's r: M=35, R=1.2, n=100

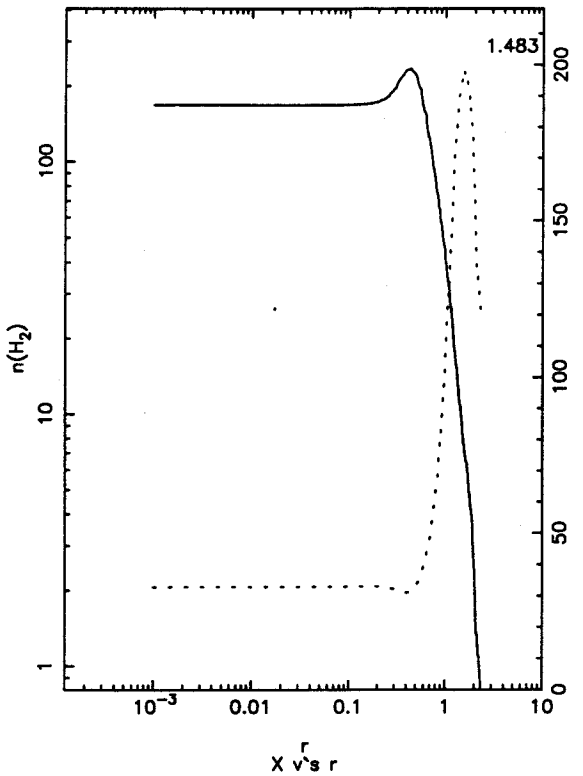

V_r v's r

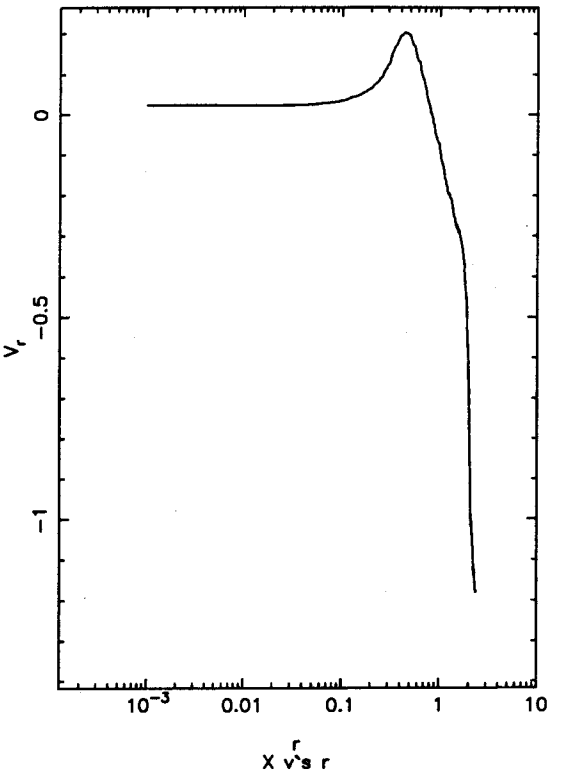

X v's r

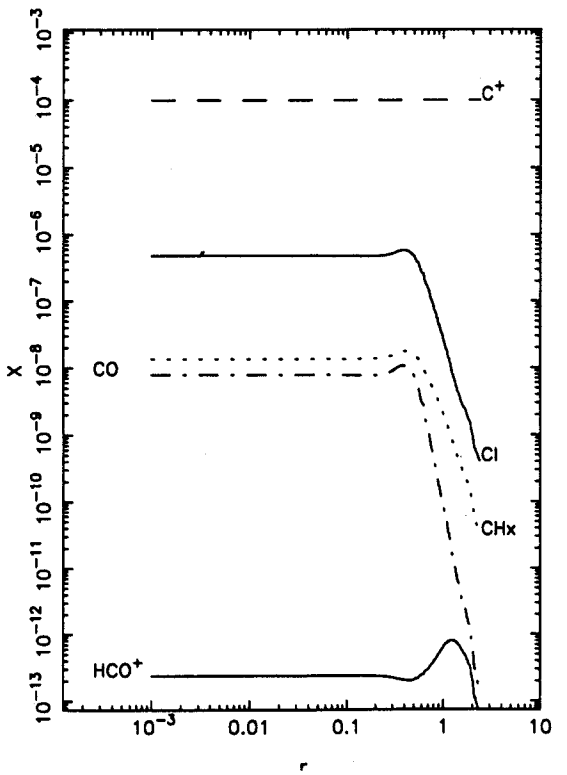

X v's r

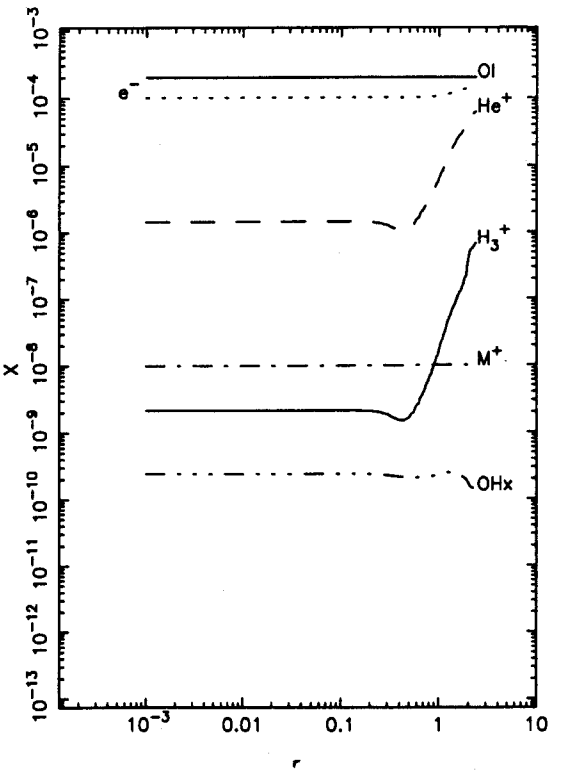

Fig. 2c – n(H2) and T v's r: M=35, R=1.2, n=100

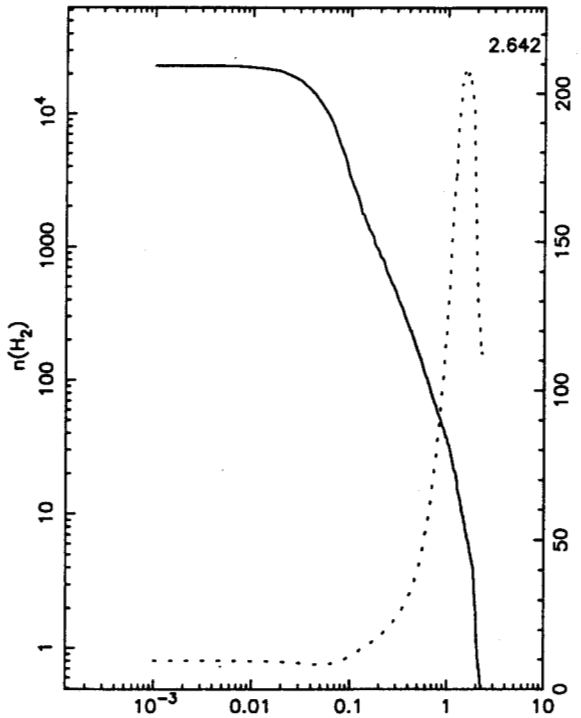

V_r v's r

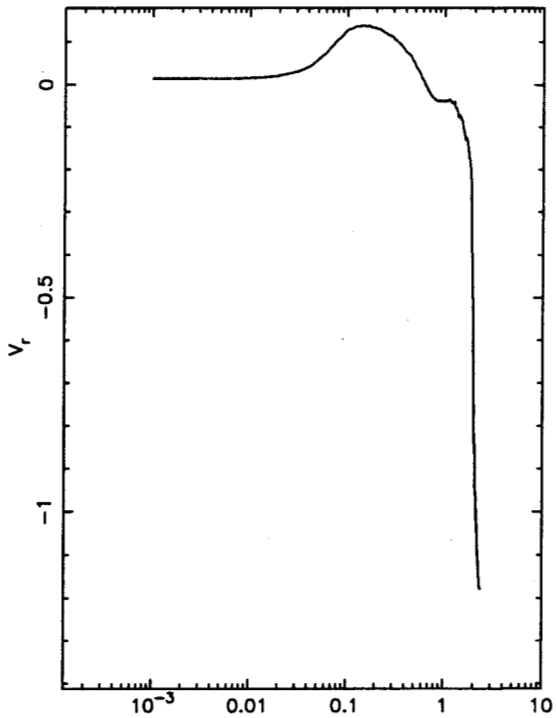

X v's r

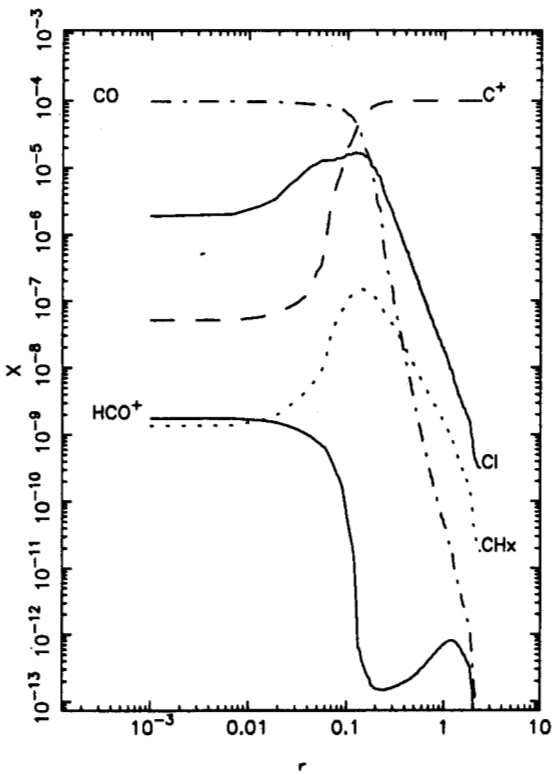

X v's r

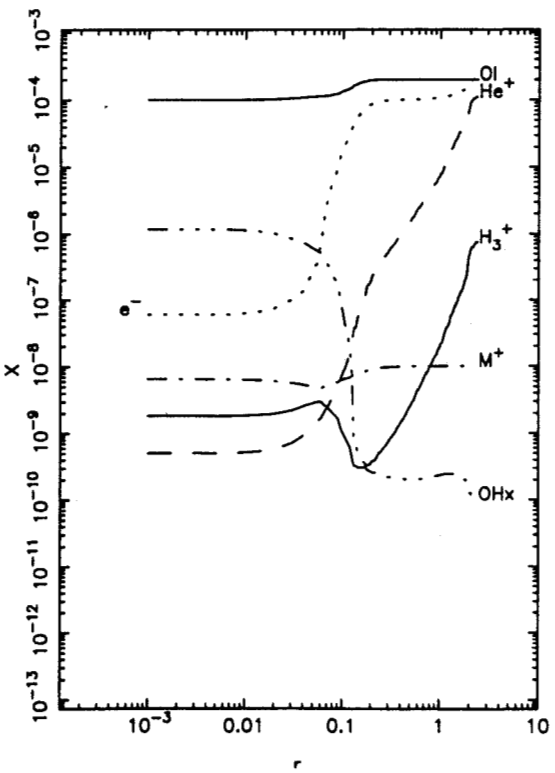

Fig. 2d – n(H2) and T v's r: M=35, R=1.2, n=100

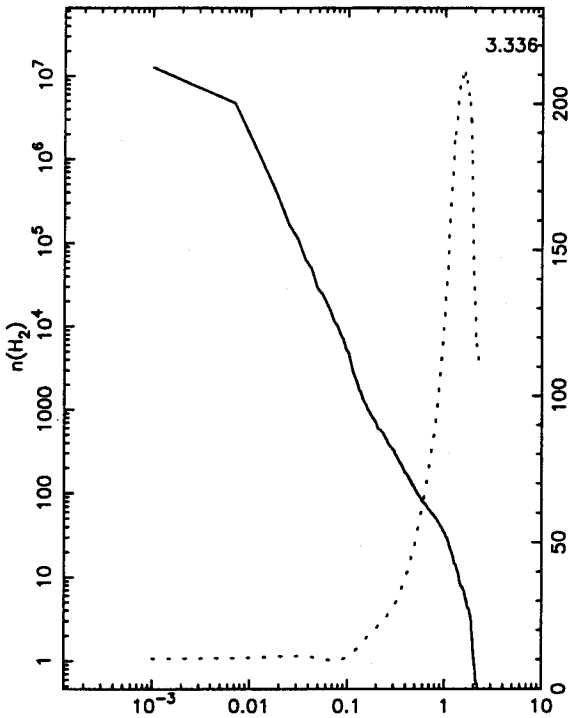

V_r v's r

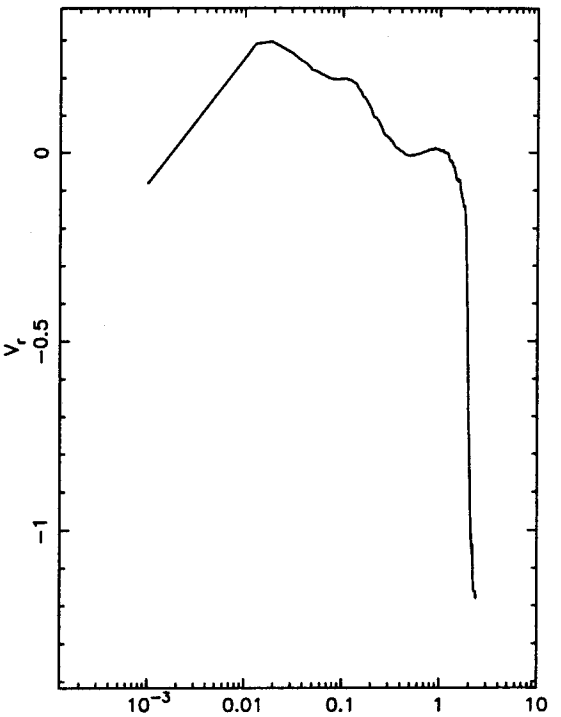

X v's r

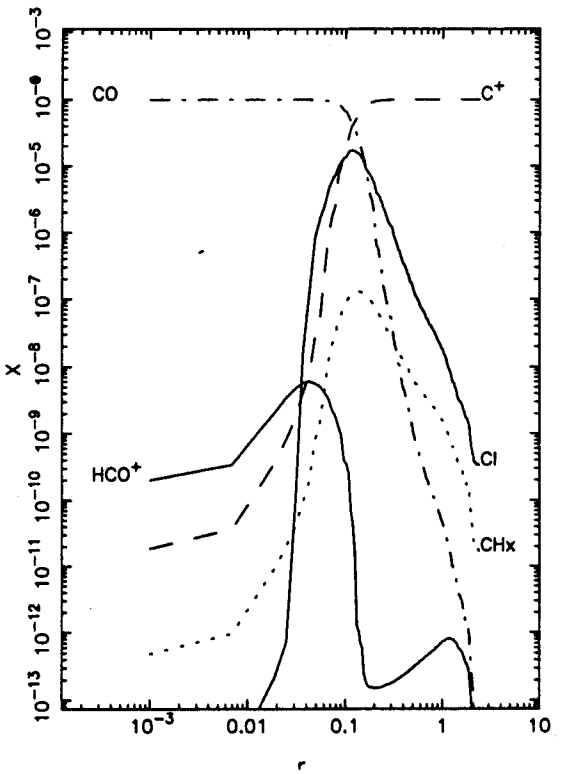

X v's r

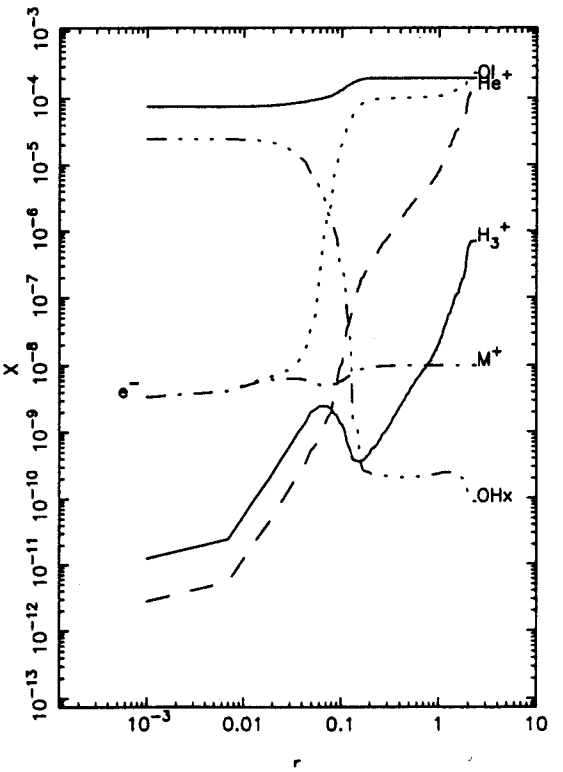

Fig. 3 – Evolution of α for different radii

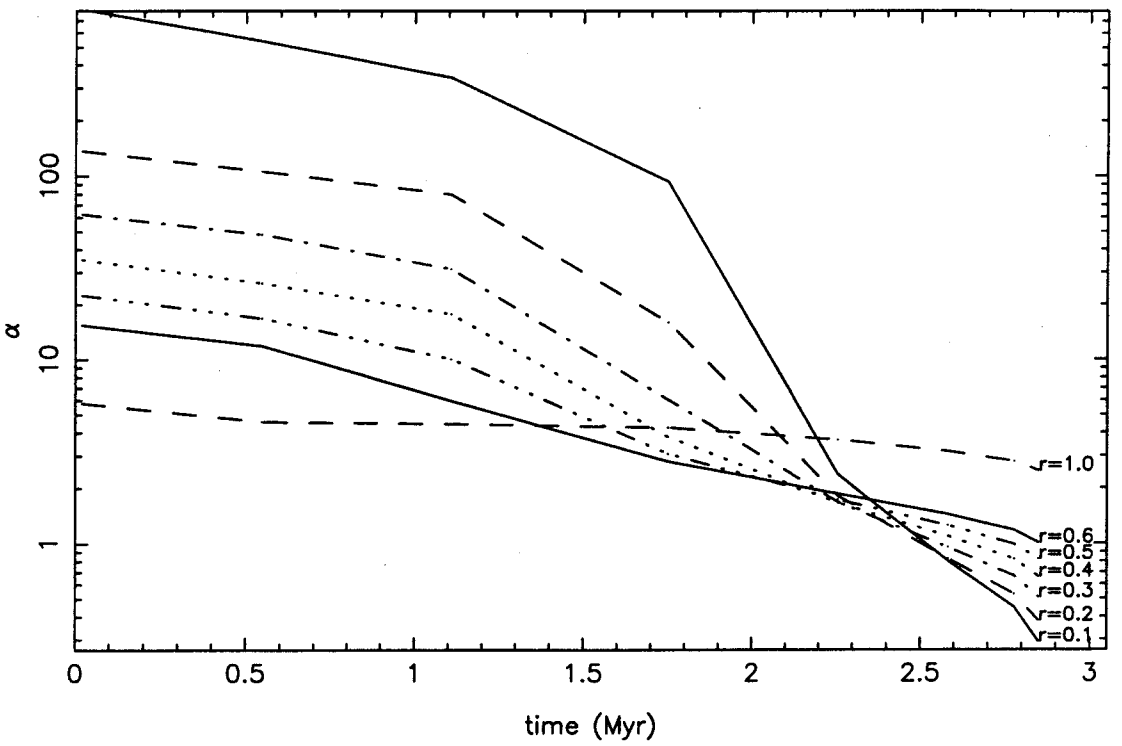

Fig. 4 – $n(H_2)$ and T v's r: M=35, R=1.2, n=100

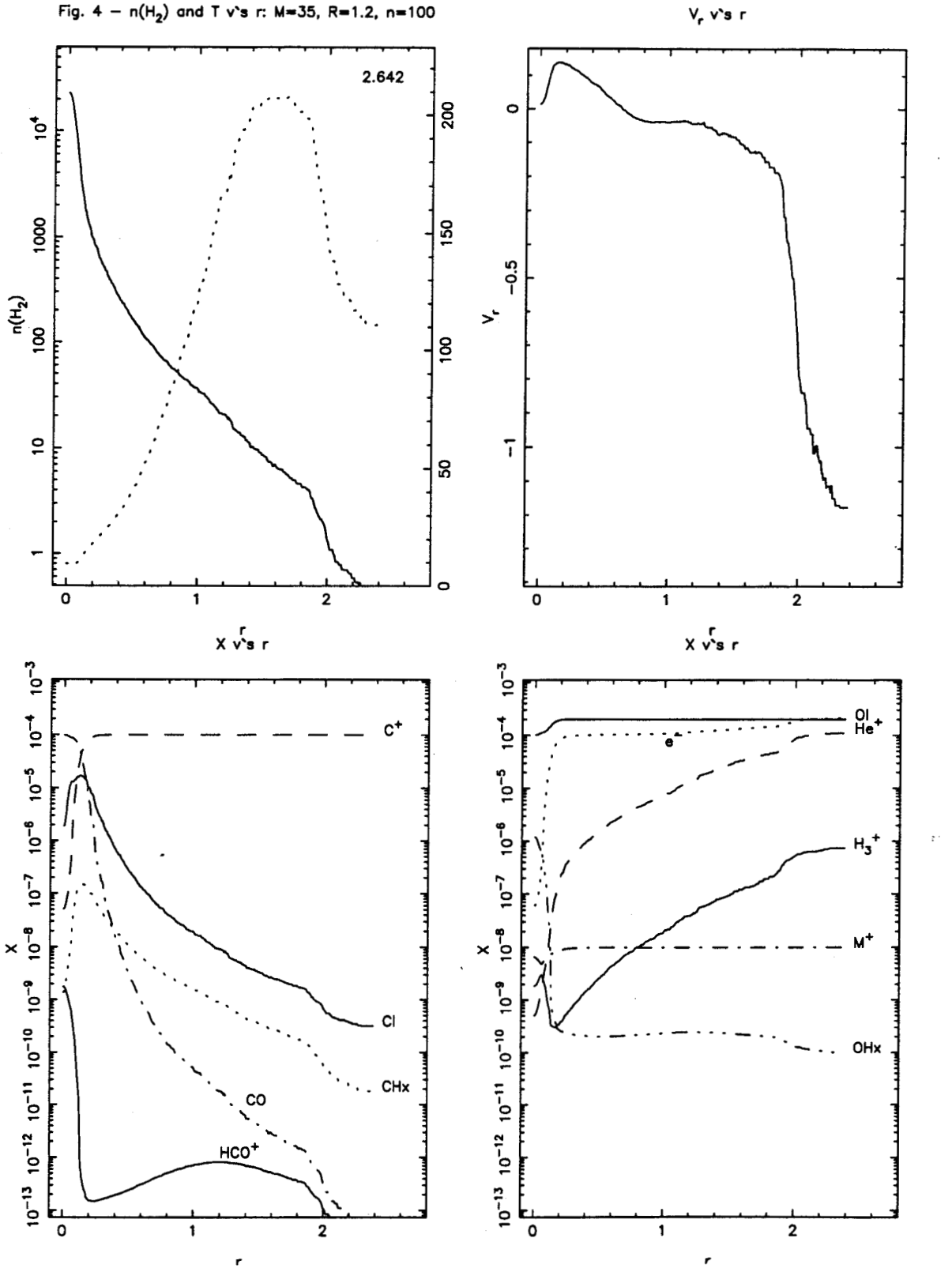

Fig. 5a – $n(H_2)$ and T v's r: M=40, R=1.25, $n=r^{-1}$

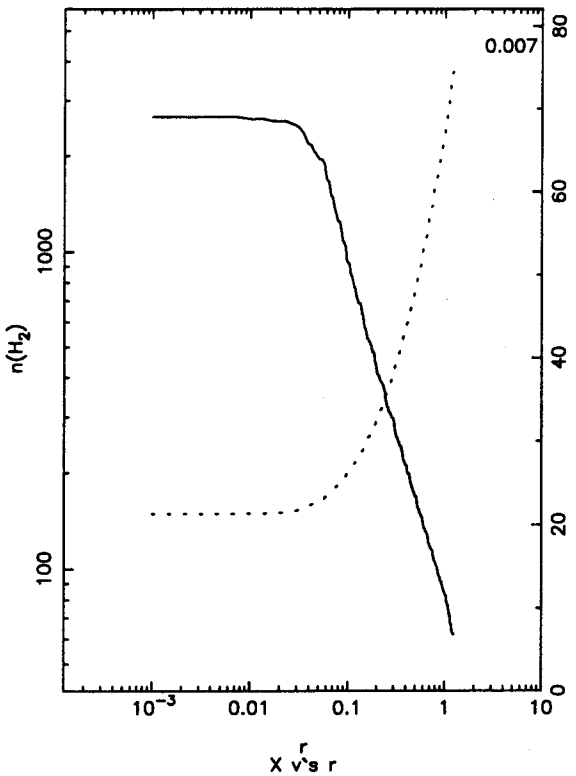

V_r v's r

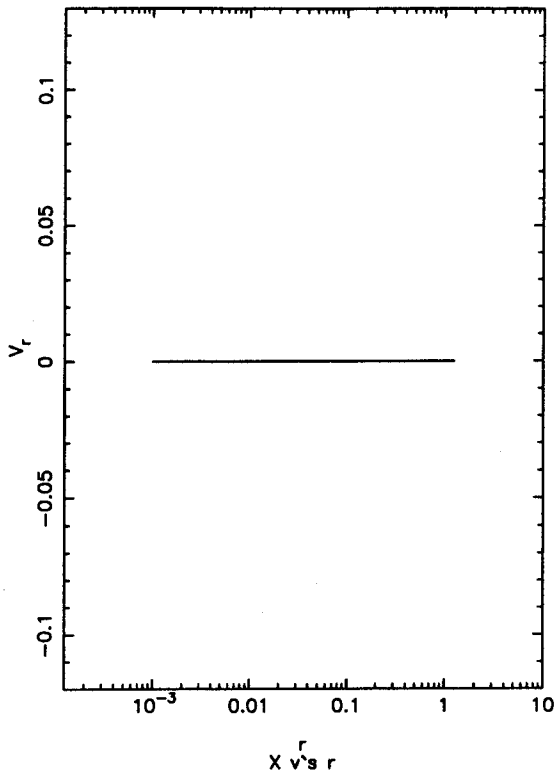

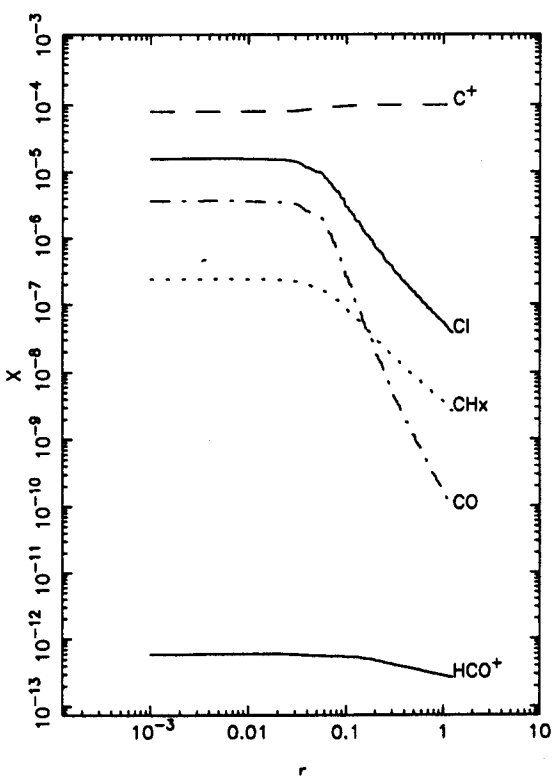

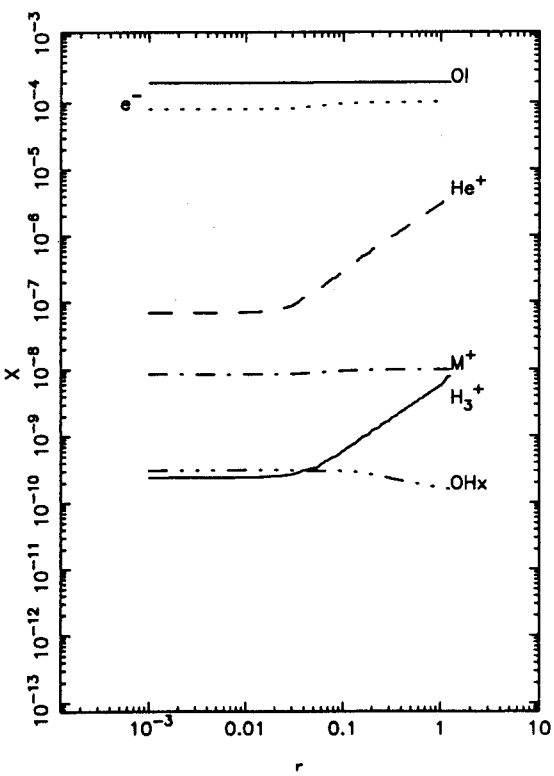

Fig. 5b – $n(H_2)$ and T v's r: M=40, R=1.25, $n=r^{-1}$

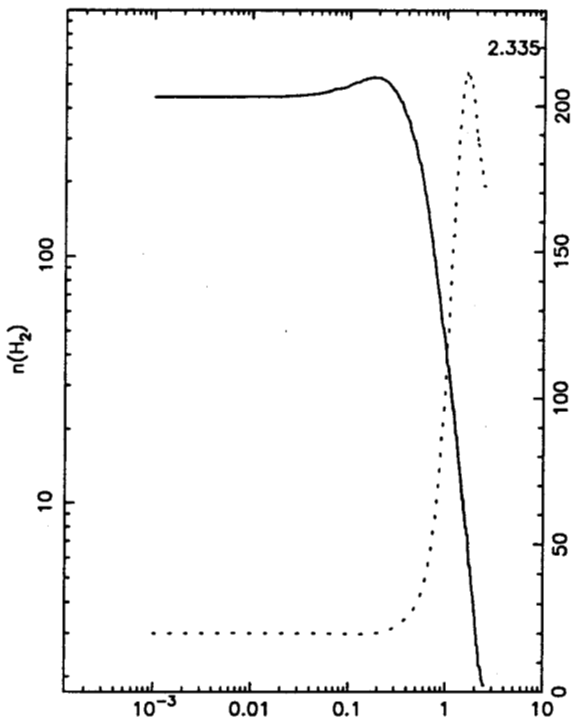

V_r v's r

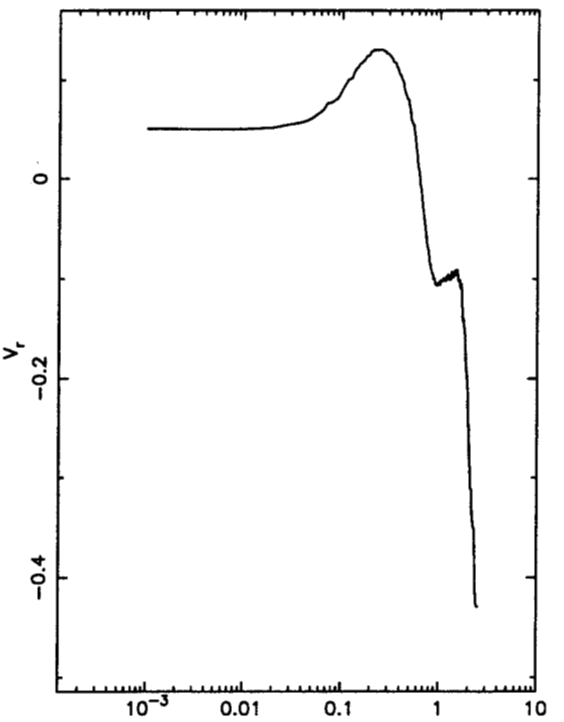

X v's r

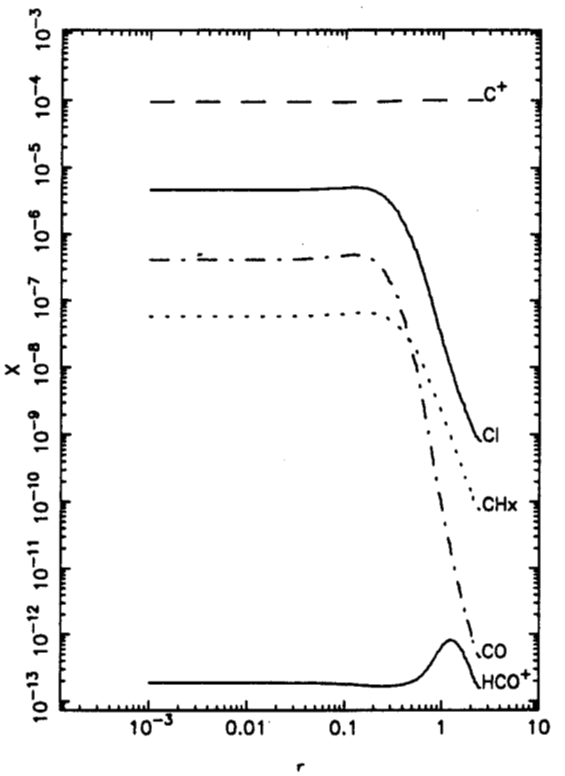

X v's r

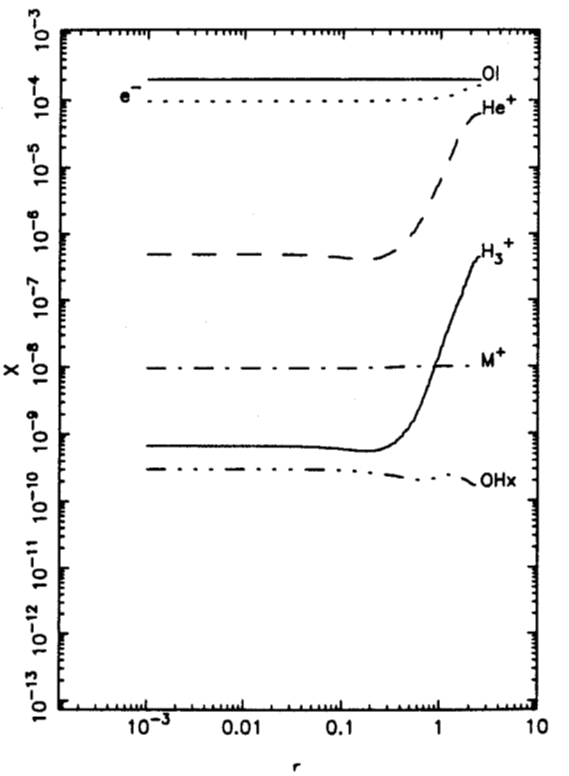

Fig. 5c – $n(H_2)$ and T v's r: M=40, R=1.25, $n=r^{-1}$

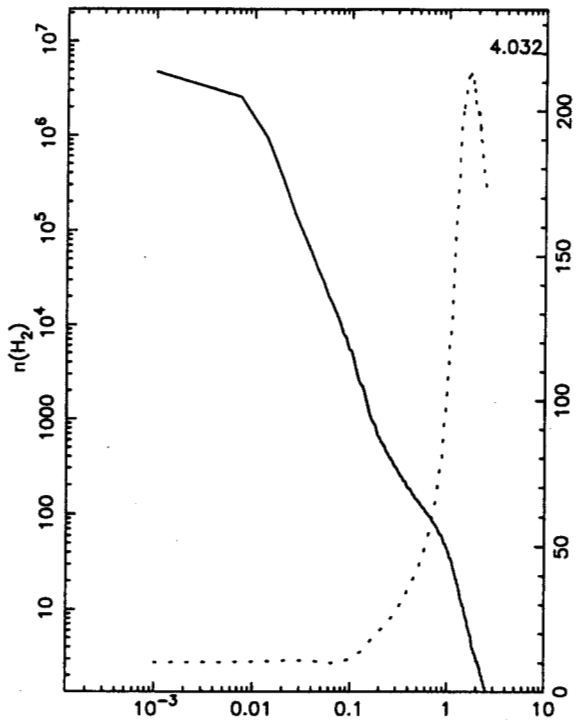

V_r v's r

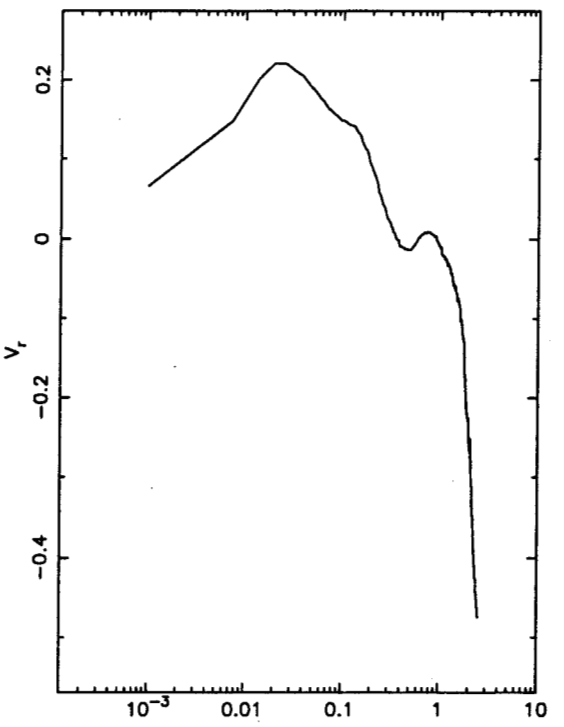

X v's r

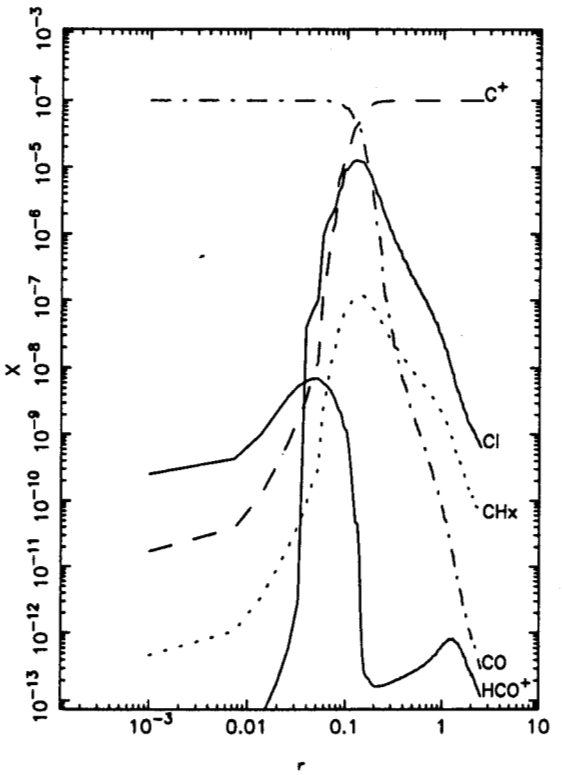

X v's r